Max-Planck-Institut für
Biogeochemie

MPI-BGC
Jena

TECHNICAL REPORTS
9

URBANIZATION IMPACTS ON THE CLIMATE IN EUROPE

by
Kristina Trusilova

ISSN 1615-7400

MAX-PLANCK-GESELLSCHAFT

Technical Reports - Max-Planck-Institut für Biogeochemie 9, 2006

Max-Planck-Institut für Biogeochemie
P.O.Box 10 01 64
07701 Jena/Germany
phone: +49 3641 576-0
fax: + 49 3641 577300
http://www.bgc-jena.mpg.de

URBANIZATION IMPACTS ON THE CLIMATE IN EUROPE

Dissertation
zur Erlangung des Doktorgrades
der Naturwissenschaften im Fachbereich
Geowissenschaften
der Universität Hamburg

vorgelegt von

Kristina Trusilova

aus Reutov, bei Moskau, Russland

Hamburg
2006

Kristina Trusilova
Max-Planck-Institut für Biogeochemie
Hans-Knöll-Str. 10
07745 Jena
Deutschland

Betreuung der Doktorarbeit durch:
Dr. Galina Churkina, *Max-Planck-Institut für Biogeochemie, Jena*
Prof. Dr. Martin Heimann, *Max-Planck-Institut für Biogeochemie, Jena*
Prof. Dr. Martin Claußen, *Universität Hamburg*
Dr. Ute Karstens, *Max-Planck-Institut für Meteorologie, Hamburg*

Unterstützende Beiträge durch:
Martin Jung

Als Dissertation angenommen
vom Department Geowissenschafter der Universität Hamburg

Auf Grund der Gutachten von
Prof. Dr. Martin Claußen
und
Dr. Galina Churkina

Hamburg, den 12. Dezember 2006
Prof. Dr. Kay-Christian Emeis
Leiter des Department Geowissenschaften

URBANIZATION IMPACTS ON THE CLIMATE IN EUROPE

Kristina Trusilova

Hamburg 2006

Abstract

This work is focused on studying urbanization effects on the climate in Europe at local and regional scales. The objectives include three topics: 1) studying impacts of urban land cover on the climate, 2) predicting impacts of different forms of urban development on the climate and 3) estimating urbanization-driven climate effects on the land carbon uptake in Europe. Numerical models of climate and terrestrial ecosystem are used to address these questions.

Effects of urban land cover on the climate are isolated using the PSU/NCAR Mesoscale Weather Prediction Model (MM5) with a modified land surface scheme based on the Town Energy Balance (TEB) model. For estimating effects of climate changes on the land carbon uptake, the Biogeochemical Terrestrial Ecosystem Model BIOME-BGC is used.

It was found that conversion from rural to urban land results in significant changes of the near-surface temperature: the diurnal temperature range in regions of land cover perturbation was reduced in average by −0.73±0.54°C in winter and −1.26±0.71°C in summertime. Inclusion of urban land resulted in a reduction of total precipitation in Europe, although urban areas alone receive more precipitation in winter (+0.09±0.16 mm day^{-1}) and less precipitation in summer (−0.05±0.22 mm day^{-1}). The study suggested that an expansion of urban area by 100% would result in an even stronger reduction of urban summer precipitation (−0.17±0.44 mm day^{-1}) and urbanized regions of Southern Europe would experience the strongest reduction.

A possible way of improving city's thermal regime by managing urban vegetation was studied for Berlin and Madrid urban areas. It was found that replacing urban grass lawns by tree stands would help to reduce the near-surface temperature by up to 1°C and to mitigate urban heat island.

The urban climate contribution to the net carbon balance in Europe was found to be rather small as compared to fertilization effects provided by urban CO_2 and NO_x pollution.

Acknowledgments

Three years I spent in Germany doing my PhD work is much more than a just *Promotion Studium*. My life has changed, my professional and personal growth made their irreversible impact on my personality and professional qualification. Many people have contributed to this directly or indirectly. It would be impossible to thank them all here because the listing would double the size of my thesis, so I just mention the closest friends and colleagues who have been with me during this unforgettable time of my life.

I would like to thank Dr. Ludmila Churkina, my supervisor at Moscow Power Engineering Institute (TU) in Moscow, where I have completed my master degree in 2003, for motivating me to move abroad and take a challenge of starting a new life here in Germany.

I thank my supervisor Dr. Galina Churkina who was with me for all these years and became more than just a supervisor and a compatriot but a friend who supported me in difficult moments of my professional life by her good advice and an encouraging word.

Dr. Ute Karstens, Prof. Dr. Martin Heimann, and Prof. Dr. Martin Claussen contributed a lot to this thesis as well being my advisory committee and helping to develop my feeble idea of the urban climate modelling into a sensible piece of work.

I would like to thank my dear friends, Elena and Robert, who spent their time with me having fun and sharing troubles. Without Elena my plants would have died from a drought and the question “What one can learn from a model?” during our looong coffee-breaks would have remained unanswered. Robert has introduced me into the German way of life with its rules and compliances, helped to learn the beautiful *Deutsch* language and to enjoy using it.

I also thank all my friends who I had a nice time with having parties, sincere talks and travelling around Europe: Birgit, Madina, Paulina, Tino, Oleg, Rona, my desperate friend Luca from Italy and my dear friend Dorothea from Erfurt who likes *syrki* and Russian language. I especially thank Jørn, who took his time to correct my writing and to translate my Runglish into the proper English, was patient with my PhD-finish-moodiness and accepted (with just a little grumbling) my vegetarian cooking.

But the people who gave me the reason and the power to pursue towards my Dr.Nat.Sc., through the B.Sc. and M.Sc. in mathematics, are my parents. My father, Victor Trusilov, has always been proud of me and helped me to keep up working by a good advice and his reassuring word. My mother, Natalya Trusilova, who in 1997 was almost terrified by her daughter’s choice of profession, provided me with a challenge to test&proof that I could go beyond the “typical-girls-job” fate of a Russian woman. My parents’ great love, which I always feel despite of the distance between us, is my source of vital energy. For this reason, I dedicate this thesis to them.

Content

1. Representation of urban land in a regional model: modification of the Land Surface Scheme in the PSU/NCAR Mesoscale Weather Predicting Model (MM5)

1.1. Introduction

Regional models in connection with increasing capacities of computers in the last few years have considerably increased the spatial (vertical and horizontal) resolution. It is common that some regional models run with a grid spacing of 5-20 km for local and regional climate analysis. On such fine scales, the influence of urban land cover on the atmospheric circulation becomes important and urban land needs to be represented in these models to capture urban weather (temperatures, humidity, and precipitation) and its effects on the boundary layer. Urban heat islands (UHI), i.e. areas where urban air temperatures are significantly higher than temperatures of rural surroundings, have large impacts on the local climate. The UHI occurs due to differences in thermal, and radiative properties of urban surface materials from the ones of natural surfaces, multiple reflection and absorption of sunlight by urban surfaces (due to specific geometry), anthropogenic heat sources and lack of evapotranspiration in urban areas (Oke, 1982). The UHI may greatly change the local climate and thus should be captured by climate models on local and regional scales.

The distinction between urban and non-urban land in regional climate models is commonly handled by modification of specific land surface parameters of a soil-vegetation-atmosphere interaction scheme. Best (2005) proposed to parameterize urban areas as bare soil surfaces and to introduce the urban land fraction for each model grid cell. Atkinson (2002) suggested to differentiate urban from rural land by setting different values to surface parameters (albedo, emissivity, roughness length, sky view factor) and to add anthropogenic heat fluxes into the model. Although these physical schemes can represent dominant impacts of urban land cover on the atmosphere, the near surface processes are insufficiently resolved. The use of only one spatially-averaged surface temperature in urban areas similarly to soil-vegetation schemes should be debatable (Masson, 2000), because it is observed that the Monin-Obukhov similarity theory, which is often used to compute the turbulent fluxes

towards the atmosphere, does not apply for temperature in the heterogeneous urban areas due to the presence of the roughness sublayer (street canyons).

Having a consistent treatment of the urban land cover in climate models will allow improving predictions of urban meteorological conditions for climate and air quality studies. This chapter focuses on improving urban land modelling for the urban area of Berlin through a modification of the land surface scheme in a regional climate model.

1.2. Materials and Methods

1.2.1. Regional model MM5

The limited-area mesoscale weather prediction PSU/NCAR model MM5 (Grell et al., 1995) was chosen for this study. This nonhydrostatic model simulates and predicts mesoscale atmospheric circulation and is typically used at regional scales of 5-50 km. The distinction between urban and non-urban areas within its land surface scheme NOAH[1] Land Surface Model (LSM) (Chen and Dudhia, 2001a; Chen and Dudhia, 2001b; Ek et al., 2003) is handled by modifications of specific land surface parameters for each model grid cell – surface albedo, roughness length, emissivity, water availability and thermal inertia (see Appendix 1).

As the model was not explicitly designed to distinguish between boundary layer and canopy layer phenomena, such as heat island or limited evaporation in urban areas, the effects of the complex urban surface on the energy balance could be parameterized only indirectly. At the horizontal spatial resolution of 10 km chosen for this study heterogeneous structure of urban surfaces, thermal and radiative properties of urban materials become important and require a more detailed representation. To account for this, the existing LSM for the urban land use type is modified using a single-layer urban canopy model of Masson (2000).

[1] **N**: **N**ational Center for Environmental Prediction (NCEP)
O: **O**regon State University (Dept of Atmospheric Sciences)
A: **A**ir Force (both AFWA and AFRL - formerly AFGL, PL)
H: **H**ydrologic Research Lab - NWS

1.2.2. Modifications of the land surface model

For this study the urban surface scheme has to be generalized in order to represent large horizontal scales (10-100 km) and to be able to capture radiative budgets, momentum, turbulent heat and ground fluxes from heterogeneous urban surfaces. In contrast to more comprehensive urban surface schemes, which include parameterisations for the canyon orientation (Kusaka et al., 2001; Martilli et al., 2002) and heterogeneous building morphology (Martilli *et al.*, 2002), the Town Energy Budget (TEB) model (Masson, 2000) includes a simplified description of the town geometry. It assumes that all buildings are of the same shape and are set on the same distance away from each other with no discretisation for the street orientation. Such generalisation allows model applicability for multiple urban areas and makes it suitable for the application on the domain in this study.

A single-layer urban canopy model (UCM), which includes TEB surface parameterisation scheme for urban non-vegetated land and LSM for urban vegetated land, is incorporated into the atmospheric model. UCM uses three urban surface temperatures, which represent temperatures for roofs, walls and roads (as in TEB) and the temperature over urban vegetated surface (as in LSM). The roof top level and the vegetation canopy top level in UCM correspond to the lowest level (surface) of the atmospheric model. At this level of the atmospheric model, the three turbulent flux contributions (from roofs, street canyons and vegetated surfaces) are averaged proportionally to their horizontal area fractions in the grid of the atmospheric model.

The UCM scheme is integrated into the MM5 model as a subroutine, which calculates the soil moisture, soil temperature, skin temperature, snow pack water equivalent and all terms of the surface energy balance and surface water balance for urban surfaces.

UCM includes explicit parameterisation for three types of man-made surfaces: roofs, roads, and walls. This makes it possible to calculate quantities of absorbed/reflected radiation by multiple surfaces and to represent the trapping of incoming direct radiation in the urban canopy. The model calculates heat and moisture fluxes from three urban surfaces (Figure 1) and fractional vegetation, includes additional anthropogenic sensible heat (H) and latent heat (LE) fluxes from the urban canopy to the atmosphere: 1) sensible heat flux from the transportation at the road level, 2) sensible heat flux and latent heat flux from industrial sources at the

roof level. Outgoing heat fluxes from urban impervious and vegetated surfaces are aggregated into energy and momentum exchange between the urban canopy and the atmosphere.

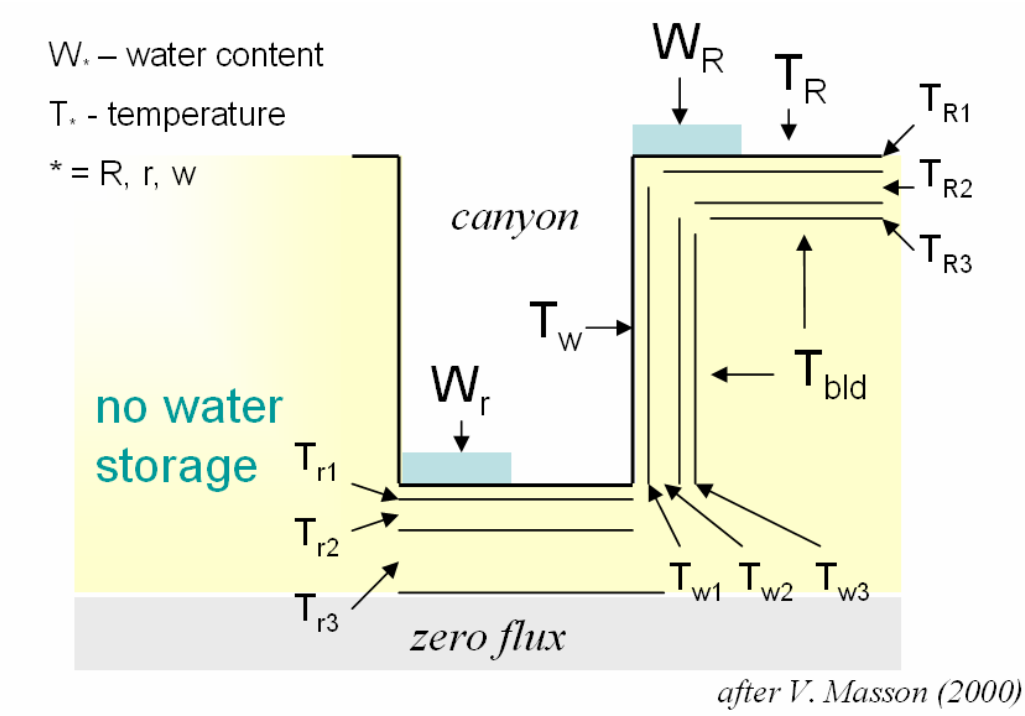

Figure 1. Discretization of the surfaces (roof, wall, road) and prognostic variables: layer temperatures T_{*k} (* = *R, w, r*; here three layers are displayed for each surface, so *k* = 1*; 2;* 3), surface water content W_* (* = *R, r*). The layer temperatures are representative of the middle of each layer. The surface temperatures are assumed to be equal to the surface-layer temperature: $T_* = T_{*k}$. The internal building temperature T_{bld} is prescribed.

The equation for temperature evolution for UCM is taken from the Town Energy Balance (TEB) scheme of Masson (2000) and includes 3-layer heat equation for inner temperatures of three different surfaces: roof, wall, and road.

$$C_{*1}\frac{\partial T_{*1}}{\partial t} = (1-\delta_{snow*})\frac{1}{d_{*1}}\left(S_* + L_* - H_* - LE_* - G_{*1,2}\right) + \delta_{snow*}\frac{1}{d_{*1}}\left(G_{*snow,1} - G_{*1,2}\right),$$

where

* - roof, road or wall;

δ_{snow} – fraction of the surface covered by snow;

d_{*1} – thickness of the surface layer;

C_{*1} – specific heat capacity of the surface layer;

S_* – net solar radiation;

L_* – net infrared radiation;

H_* – sensible heat flux;

LE_* – latent heat flux;

$G_{*1,2}$ – conduction heat flux between the surface layer and the underlying layer;

$G_{*1,snow}$ – conduction heat flux between the snow layer and the surface;

$$C_{*k}\frac{\partial T_{*k}}{\partial t}=\frac{1}{d_{*k}}\left(G_{*k-1,k}-G_{*k,k+1}\right), k=1,..n\,,$$

where

n – number of layers for roof, road, and wall, n=3;

d_{*k} – thickness of the layer k;

C_{*1} – specific heat capacity of the layer k;

$G_{*k\text{-}1,k}$ – conduction heat fluxes between the *k-1* and k layers;

$G_{*k,k+1}$ – conduction heat fluxes between the k and *k+1* layers;

The coupled MM5-UCM system uses a single urban land class as input, which is characterized by a set of parameters.

The Berlin urban area was chosen for this study because the most recent observation data of near-surface temperatures and precipitation, which are representative for the total urban area or its large parts, are freely available and can be used for a corroboration of the model results.

Thermal and radiative properties of urban roofs, walls, and roads are set to the values as in the work of Oke (1988) and Masson (2000)(see Appendix 2), assuming that all buildings have the same size, are set apart from each other on an equal distance, and are made of the same materials. Thus, the average height (h) and aspect ratio of buildings (h/l, where l – building's width) as well as the aspect ratio of the street canyon[2] (h/w, where w – width of a street) are set to represent the urban area of Berlin (Table 1).

The limited surface evaporation in the UCM is represented through the limited maximum water-holding capacity of 1 kg m^{-2} water for roof and road surfaces, while the water-holding capacity of walls is set to zero. The excess of water is lost as runoff. These roofs and roads are impervious, but a certain fraction of each of them may be

[2] *canyon* - a road bordered by two facing building walls (after Oke T.)

covered by water immediately available for evaporation, while the rest of the surface is assumed to be dry.

Table 1. Parameters for the urban canopy model for the Berlin urban area.

Symbol	Designation of symbol	Value	Units
a_{town}	Fractional area occupied by artificial materials	0.69	-
a_{bld}	Fractional area occupied by buildings	0.54	-
H	Average building height	20.0	m
L	Average building width	20.0	m
h/l	Building aspect ratio	1.00	-
W	Average street width	20.0	m
h/w	Canyon aspect ratio	1.00	-
$z0_{town}$	Roughness length for canyons	2.00	m

The fraction of vegetation cover of the urban canopy is calculated from available data (Hupfer and Chmielewski, 1990; Lavalle et al., 2002) and set to 0.23 representing the urban area of Berlin.

The urban canopy model described here is not a copy, but a simplification of the above mentioned TEB. UCM includes the surface parameterisation, prognostic equation for the temperatures of 3-layer urban materials and the representation of the water surface runoff as in the TEB. However, the UCM makes use of the standard LSM model for vegetated areas.

1.2.3. Modelling protocol

To compare effects of the two urban land parameterisations in the standard LSM surface scheme and the UCM composite model, two corresponding model simulations are performed on the domain which includes Berlin urban area. The first simulation is performed with the standard LSM land-surface model and is denoted OLDU. The approach used in OLDU for representing urban land is based on the soil-vegetation-atmosphere interactions scheme, where urban land is represented similarly to the "barren soil" or "desert" land use type of the LMS. The second simulation is performed with the coupled UCM land-surface scheme and is denoted as NEWU. In

both simulations the unmodified LSM is used for non-urban land use types, while in NEWU the modified UCM model is used for urban pixels.

The model domain of 34x34 grid cells includes the urban area of Berlin (Figure 2) and its surroundings with the grid size of 10 km and has 23 vertical σ-levels. It is nested in an intermediate domain with a 30 km spatial resolution to avoid boundary effects from the lateral meteorological fields. The simulations are run over one month, July 2005. The model is driven at the lateral boundaries by the NCEP Final Analysis dataset[3] on the one-degree spatial resolution. The forcing at lateral boundaries is applied every 12 hours, at 00:00 and 12:00 of each simulated day. An additional boundary condition needed for the urban canopy model, the internal temperature of buildings, is set to the constant of 20°C.

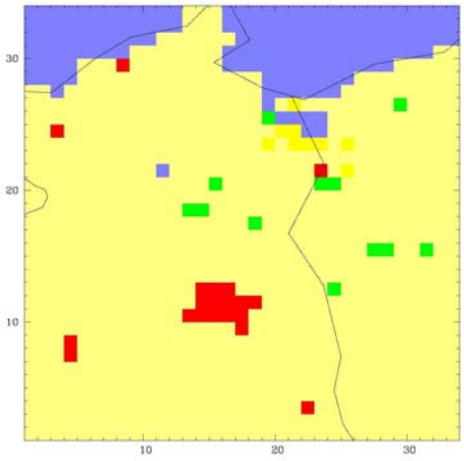

Figure 2. Berlin urban area (in red) is situated at 52°31'N 13°24'E and surrounded by extensive croplands or grasslands (yellow) and sparse forests (green).

For the model setup, a simple single-cloud cumulus parameterisation scheme is used. In this scheme, which is typically used in MM5 model on the spatial resolution of 10-30 km, clouds are represented as one updraft and one downdraft fluxes (Grell *et al.*, 1995). For parameterisation of non-liquid precipitation the simple ice scheme of Dudhia (Dudhia, 1989) is used. This scheme allows no supercooled clouds and immediate melting of snow below melting level (no supersaturated and supercooled clouds). For the planetary boundary layer parameterisation the medium-range forecast scheme (MRF PBL) of Hong and Pan (1996) is used. The mentioned above

[3] FNL ds083.2, dss.ucar.edu/datasets/ds083.2/data/

parameterisation schemes are included into the standard version 3.7 of the MM5 model.

In the UCM scheme, to account for anthropogenic influence in the calculation of the canyon temperature and humidity, the anthropogenic heat sensible flux due to traffic is added at the road level. The small anthropogenic sensible heat flux and latent heat flux due to industry are added at the roof level for the calculation of the turbulent fluxes at the town scale (Table 2). The values of fluxes are taken from the work of Masson (2000).

Table 2. Anthropogenic heat fluxes in UCM.

Variable	Designation	Flux (W m^{-2})	Model level, where flux is assigned
H_{traf}	sensible heat flux due to traffic	40.0	road
H_{ind}	sensible heat flux due to industry	5.0	top of canyon
LE_{traf}	latent heat flux due to traffic	0.0	-
LE_{ind}	latent heat flux due to industry	5.0	top of canyon

For the non-urban surfaces the standard LSM land surface scheme is used, while for urban surfaces the UCM subroutine is called. This scheme is used to calculate the surface fluxes into the PBL scheme and as a diagnostic equation to calculate the skin temperature and the near-surface temperature at 2 m above ground. Radiative and thermal properties of the vegetation cover (albedo, roughness length, emissivity, thermal inertia etc.) remain fixed through all simulations; changes of these properties due to vegetation dynamics are not included into the standard LSM. The soil temperature and moisture content fields for model initialisation are available from NCEP Final Analysis dataset at four levels of 0.1, 0.4, 1.0, and 2.0 m from 2005 in contrast to the poor representation of the data at 0.1 and 2.0 m levels only in the dataset from earlier years.

Previous investigations revealed that the strongest differences between urban and rural temperatures, e.g. strong UHI, as one of the major urban perturbations of the environment, may occur in winter (Montavez et al., 2000) and in summer (Bottyan et al., 2005; Unger et al., 2001). Given the large computational costs of the model runs over the full domain, the calculations are restricted to the snow-free period when

urban surfaces are open to the atmosphere and significant effects of the urban land on the climate are expected. Thus, July of 2005 was chosen for the simulations.

1.3. Results and Discussion

1.3.1. Simulation of surface energy balance by the standard LSM and the modified urban land surface scheme UCM

The representation of three urban surfaces (roof, road, and wall) results in strong effects on the surface energy balance (Figure 3). Roofs, roads, and walls parameterized in UCM (NEWU-simulation) have different thermal properties (heat capacity and thermal conductivity) and surface radiative properties (albedo and emissivity) from the urban land use type in LSM (OLDU-simulation). For more information see Appendix 1 for LSM and Appendix 2 for UCM. The low albedo of roads (0.08) and roofs (0.15), which results from the dark colour and shading, provides a larger fraction of incoming sunlight absorbed by these surfaces in contrast to the higher albedo (0.18) of the urban land use category used in the standard LSM. The high emissivity of roads (0.94) leads to a smaller fraction of the direct sunlight being reflected back to the atmosphere as compared to the emissivity of LSM urban land (0.88). These differences result in the higher ground storage heat flux density (Q_S) in NEWU-simulation (Figure 3, blue line). According to OLDU-simulation Q_S reaches its maximum at 9:00-12:00 and then gradually declines until at 17:00 it changes its direction from heat accumulation to heat release. The ground flux Q_S in NEWU-simulation is generally higher throughout the day, it reaches maximum at 12:00 (or later) and then, after the sun has passed its apogee, rapidly declines until 18:00. However, the heat release to the atmosphere (reverse of the flux) happens several hours later, around 21:00.

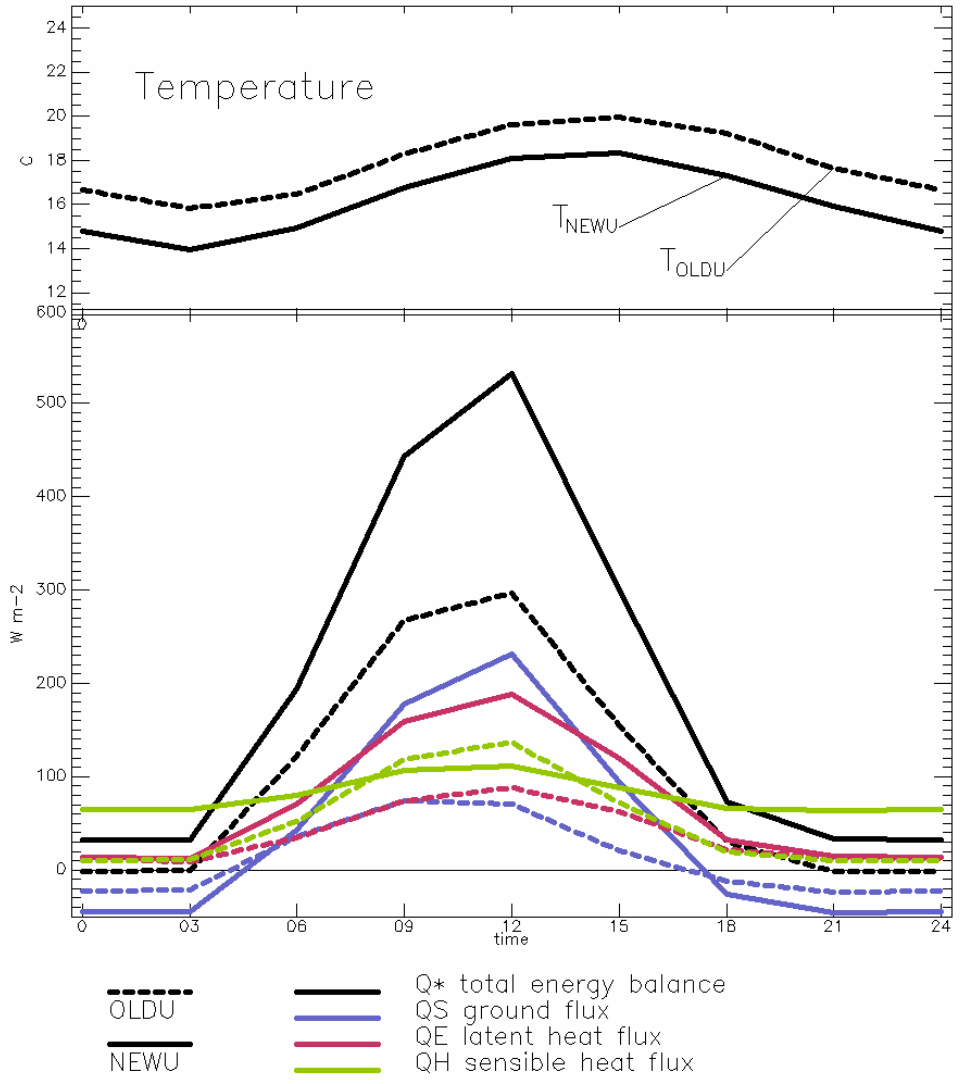

Figure 3. Synchronous energy balance and near-surface temperature of an urban site simulated by the MM5 model with standard LSM (dashed lines) and coupled UCM (solid lines). The fluxes are averages over the simulation of 30-day in July 2005.

The energy balance is also affected by the lack of infiltration in urban areas, which prevents water storing for later evapotranspirative cooling and is reflected in the high latent heat flux density (Q_E) in the NEWU-simulation (Figure 3, red line): the fraction of precipitated water which stays on the ground (not runoff into the drainage system) is available for immediate evaporation which is enhanced by the higher urban surface temperatures. In the standard LSM, urban land is parameterized similarly to the barren ground by setting the low surface moisture availability parameter (0.02). In urban areas, the large fraction of rain water is lost into the drainage system and is not

available for evaporation. Thus, the latent heat flux is expected to be low (it is indeed, during night time (Figure 3)). However, the layer of water held on the surface is available for immediate evaporation and in case of frequent rains, it causes the latent heat flux to increase during daytime. The NEWU-scenario captures this city-specific variation of the latent heat flux.

Large numbers of people inhabit urban areas and demand for heat/power generation for different kinds of their activities (transportation, air conditioning, industries) making an important contribution to the surface energy balance. The outgoing longwave radiation (sensible heat flux density Q_H) in the standard LSM model is a fraction of the incoming solar radiation and is calculated from soil moisture content, thermal, and radiative properties of the urban canopy. In the UCM model, additional anthropogenic heat fluxes from industry and transportation are included. However, the released energy from the transportation does not go directly to the atmosphere but is absorbed/reflected by roads and walls. This effect is called "radiation trapping" and it is captured by the NEWU-simulation (Figure 3, green line): the energy is accumulated during the day (ground flux) and is released at night thus rising the temperature of the air. The contribution of anthropogenic heat sources from traffic and industries is relatively minor in summer; however its effects are seen in the diurnal variation of the sensible heat flux density (Q_H). In the day hours the Q_H in NEWU-simulation is slightly higher (80.5-111.6 W m^{-2}) than in the OLDU-simulation (52.2-136.9 W m^{-2}), but in the night hours it is significantly higher in NEWU-simulation (63.3-66.3 W m^{-2}) than in the OLDU-simulation (10.0-19.4 W m^{-2}). The latent heat flux (Q_{LE}) is higher in the urban area than in the rural area throughout the day and night time (Figure 3). This is explained by the enhanced evaporation of the available in excess moisture forced by the urban high surface temperatures.

1.3.2. Simulation of near-surface temperature by the standard MM5-LSM and MM5-UCM models

The simulations of the near-surface temperature with two land surface schemes show clear differences (Figure 4) in the surface energy balance. These differences result in the lower urban temperatures predicted by the UCM model.

Only few data sources provide observational/reanalysis data, which are representative for the urban area of Berlin or its extensive parts. The observational data for the validation of the model were collected from the following available data sources: 1) RTL Wetter database[4], 2) WetterOnline GmbH[5], 3) Urban Climate Homepage[6]. The city of Potsdam is situated south-west of Berlin in its close vicinity and is included into the metropolitan area of Berlin. This assumption makes it possible to include available observational data for Potsdam into the analysis. The data are available as average monthly maximum and minimum temperatures.

The measurements of the maximum daily temperature, taken at two airports and built-up areas of Berlin and Potsdam have high variability in time series and are not representative for the daytime temperature variation. The airport temperatures are measured over open spaces with low albedo and are influenced by the high additional heat flux due to transportation, whereas the temperatures in the unstable mixing atmosphere over build-up areas (with high roughness and low sky view factor) is expected to be lower. Indeed, among taken observations the measured maximum daily temperatures (23.3°C-23.9°C) were registered over spaces exposed to the direct sunlight and thus, the day-time observations cannot be used to validate temperatures predicted by the UCM model, which are aggregated over heterogeneous areas: roofs exposed to the direct sunlight, completely shaded and partly shaded street canyons, vegetated areas. However, the night-time measurements taken in the stable atmosphere conditions are considered representative for the urban canopy night temperature: in the absence of partial shading, surface temperatures are distributed more uniformly in the night hours than during day.

The observations of the minimum night temperature from five sites in the Berlin urban area are used for comparison with the model simulation of the diurnal temperature (Figure 4). The mean observed minimum night temperature in July 2005 is 14.5±1.1°C. The mean minimum night temperature predicted by LSM model and LSM-UCM model is 15.8±2.6°C and 13.9±2.6°C, respectively. The night temperature predicted by the LSM model is by ~1.3°C higher than the observed value, while the night temperature predicted by the UCM model matches the observation within its uncertainty range during the time interval 21:00-06:00 h (night hours).

[4] www.wetter.de
[5] www.wetteronline.de
[6] www.stadtklima.de

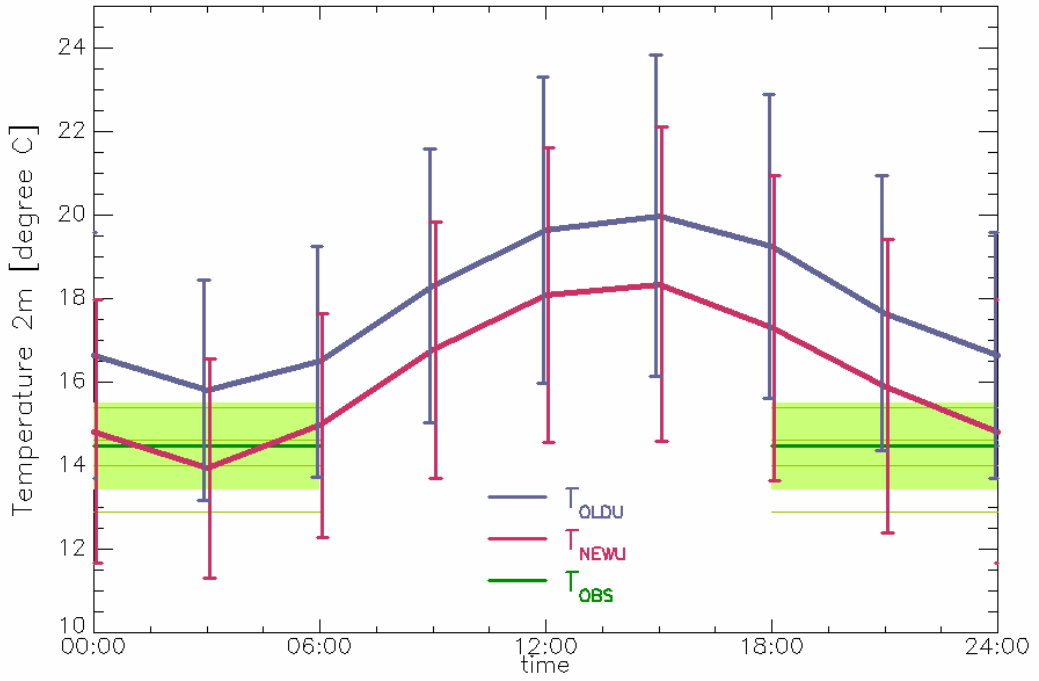

Figure 4. Near-surface temperature (at 2m) simulated by the standard LSM (OLDU) and by the coupled UCM (NEWU). Data is 30-day average over the simulation for July 2005. The green solid line and the light green polygon represent the mean and the standard deviation of the available observational data in Berlin urban area (Tempelhof and Schoenefeld airports, Berlin and Potsdam built-up areas).

Comparison of the mean minimum night temperature predicted by the LSM and UCM models to the available observational data shows that the LSM model overestimates the minimum night temperature, while the UCM provides a more realistic estimation of the nigh time temperatures.

No observation was available to validate components of the surface energy balance predicted by the models. The validation of the heat fluxes over urban surfaces for the Town Energy Balance model, which was taken as the basis for the temperature evaluation within the UCM model, was done for four urban areas in the work of Masson (2000) and in the work of Masson et al. (2002).

1.4. Summary and outlook

The simulations of the surface energy balance of the Berlin urban area with the standard LSM and the UCM land surface schemes showed that both models capture diurnal variations of the latent and sensible heat fluxes, as well as of the ground heat

flux. The ground heat flux diurnal variation predicted by the UCM model differed from the one predicted by the LSM model in the phase and indicated a three hours longer time of the heat accumulation in the ground (canopy) and a delay of the night time heat release. This shift in the phase of the ground heat flux predicted by the UCM model resulted from the radiation trapping within the urban canopy and the slow urban cooling in the night hours, which were captured by the UCM.

The comparison of the near surface night temperature predicted by LSM and UCM models to the available observations showed that the UCM model provided a better match within the uncertainty range.

The LSM-TEB composition coupled into the UCM model for urban land use was able to represent the near surface night temperatures better than the standard LSM model. The UCM includes the direct parameterisation for the anthropogenic heat flux, buildings' geometry, and the fractional vegetation cover, which makes the model applicable for multiple urban areas without changing thermal and radiative properties of urban artificial surfaces (roads, roofs, and walls). Only few additional parameters are needed for the UCM model, as compared to the standard LSM model.

The implemented modifications of the land-surface scheme resulted in a low additional computation cost of about 9 % and can be used for regional scale studies with multiple urban areas.

The flexibility of the UCM model and its relatively low demand for additional computation time make it suitable for studying local and regional impacts of urban land on the climate.

2. Effects of urban land modifications on precipitation and near-surface temperature in Europe

2.1. Introduction

Urbanization is one of the most evident examples of human modification of the Earth. The urban land cover accounts for less than 2% of the Earth's land area, but this proportion is growing rapidly as more cities expand into natural ecosystems and agricultural areas. According to the United Nations Information Service (UNIS), the proportion of the population living in urban areas is still expected to increase to 82% by 2030. However, our understanding of the role, which urbanization plays in Earth-climate system processes, is incomplete. Recently several issues rose which refer to the urban-environment+climate system linkage. One among those is "How are land use and land cover linked to climate and weather?" (Shepherd and Jin, 2004).

The landscape alteration through urbanization involves the transformation of the radiative and aerodynamic characteristics of the land surface and results in changes of the water cycle and planetary boundary layer. Several studies focused on different aspects of urban environments and their influence on climate: variable patterns of extreme temperatures within urban areas (Bernatsky, 1982; Ca et al., 1998; Gonzalez et al., 2005; Huang et al., 1987; Jauregui, 1991; Jin et al., 2005); urban heat island (Atkinson, 2002; Borghi et al., 2000; Brunetti et al., 2000); contributions of urban environments to global warming (Jones et al., 1990; Kukla et al., 1986; Parker, 2004; Wood, 1988); high CO_2 emissions over urban areas (Idso et al., 2001; Koerner and Klopatek, 2002); changes of precipitation (Dixon and Mote, 2003; Huff and Changnon Jr., 1973; Rosenfeld, 2000; Shepherd et al., 2002); reduced air moisture and evaporation in cities (Grimmond and Oke, 1999; Mayer et al., 2003). Most of these studies investigated effects of individual urban areas on local climates, while little is known about impacts of urbanization at the regional scale, where many policy makers traditionally operate, within and beyond urban land. In the present study, an attempt to investigate regional climate impacts of multiple urban areas is pursued.

Kalnay and Cai (2003) analysed surface temperature observations from 1950-1999 in the continental United States. The authors suggested that the half of the observed

reduction of the diurnal temperature range is caused by land use changes (including urbanization) and these land use changes contribute to the mean surface warming by 0.27°C per century. However, this study was unable to separate effects of urban land cover change from effects caused by changes in other land use types since this requires observations in somewhat unrealistic conditions: before and after urbanization. Due to difficulties to make such observations, a modelling approach to estimate effects of urbanization on the regional climate can be used.

Lamptey et al. (2005) explored climatic effects of urban and agricultural land cover transformation in the North-eastern United States using a regional modelling approach. The authors found that due to the land cover change in urban sites the near-surface temperature increased by 0.8 K in summer and by 1.0 K in winter on average. However, the authors performed model simulation on coarse 36 km scale and used a very simple parameterization to represent urban land.

In this chapter impacts of the urban land use in Europe at local and regional scales are examined with a regional model, which includes a modified land surface scheme for a more detailed representation of urban land at the spatial scale of 10 km. Differences in near-surface temperature and precipitation between two different states of urbanization, a hypothetical situation when no urban area is present, and the present day (2000-2005) urban land, are quantified.

2.2. Materials and Methods

2.2.1. Regional model MM5

We use the limited-area numerical weather prediction mesoscale PSU/NCAR model MM5 (Grell et al., 1995) for simulations. This nonhydrostatic model simulates and predicts mesoscale atmospheric circulation and is typically used at regional scale. The distinction between urban and non-urban areas within its land surface scheme, which is based on the community Noah Land Surface Model (LSM) (Chen and Dudhia, 2001a; Chen and Dudhia, 2001b; Ek et al., 2003), is handled by modifications of specific land surface parameters. Although the physical schemes of the model can represent dominant impacts of urban land cover on the atmosphere, the near surface processes are insufficiently resolved. As the model was not explicitly designed to distinguish between boundary layer and canopy layer phenomena such as

heat island or limited evaporation in urban areas, the effects of the complex urban surface on the energy balance could be parameterized only indirectly. At the scale of present interest (10 km), geometrical properties of the urban canopy, thermal and radiative properties of heterogeneous urban materials become important. To account for this, the existing land surface scheme is modified for the urban land cover type using a single-layer urban canopy model of Masson (2000).

2.2.2. Modifications of the land surface model

For this study the urban surface scheme has to be generalized in order to represent large horizontal scales and to be able to capture radiative budgets, momentum, turbulent heat and ground fluxes from heterogeneous urban surfaces.

A single-layer UCM described in detail in "1.2.2. Modifications of the land surface model" on page 3, which includes TEB surface parameterisation scheme for urban non-vegetated land and LSM for urban vegetated land, is incorporated into the atmospheric model.

The coupled MM5-LSM-UCM system uses one urban land use class as input, which is characterized by a set of parameters. When only a particular urban area is considered, the parameters could be set to represent its specifics e.g. built-up density, building height, vegetation fraction etc. Problems occur when multiple heterogeneous urban areas are included into the study domain: none can be parameterized individually because such information is difficult to collect and to incorporate into the model, but an average parameterisation for all urban areas is applied uniformly. In this study the thermal and radiative properties of urban roofs, walls and roads are set for all cities to values as in the work of Masson (2000).

The water reservoir of the urban canopy in UCM has a small capacity (1 kg m^{-2} for roofs and roads), and the water in excess from roofs and roads is "lost" as runoff. These surfaces are impervious and impenetrable for water, but a certain fraction of each of them can be covered by water immediately available for evaporation, while the rest of the surface is assumed to be dry.

Geometrical properties such as building height, building aspect ratio, and canyon aspect ratio as well as the fraction of vegetation cover of urban areas are averaged over available data (Lavalle et al., 2002) and set to values representing a typical middle-size European city (Table 3). The uniform parameterisation of the urban

canopy for all urban areas represents main impacts of urban land to the atmosphere and allows us to analyse the sensitivity of those impacts to different climate conditions and city sizes. However, it also might be a source of large uncertainties in the weather prediction.

Table 3. Parameters for the urban canopy model represent a typical middle-size city in Europe. The parameter values are used for all urban areas in Europe uniformly.

Symbol	Designation of symbol	Value	Units
a_{town}	Fractional area occupied by artificial materials	0.85	-
a_{bld}	Fractional area occupied by buildings	0.50	-
H	Average buildings height	20.0	M
h/l	Building aspect ratio	1.0	-
h/w	Canyon aspect ratio	1.0	-
$Z0_{town}$	Roughness length for canyons	2.0	m

2.2.3. Mapping urban areas

Two land cover maps were created to represent different states of urbanization: 1) a land cover map that includes no urban area (NOU) and 2) a land cover map with the present day distribution of urban areas (URB). The NOU-land cover map was derived by replacing urban pixels with the dominating land cover of neighbour pixels. For the present state of urban mask, a new map had to be produced since the GLCC-USGS[7] land use classification (Loveland et al., 2000) commonly used in MM5 strongly underrepresents urban areas in Europe (Figure 5a). Several available data sets were used in order to refine the spatial distribution of the cities.

The EU-CORINE[8] land cover database derived from higher resolution satellite imagery (Landsat) has a spatial resolution of 250 m and has a detailed representation of urban land. However, this database covers only a part of Europe and cannot be used as an input for the model directly. CORINE was used as a reference to evaluate existing global land cover classifications. Statistical and visual comparison between

[7] Global Land Cover Characterization from U.S. Geological Survey
[8] Coordinated Information on the European Environment from Europe Environment Agency

CORINE and GLCC, GLC2000[9] and the MODIS[10] land cover products revealed that none of them captures urban areas in Europe well enough.

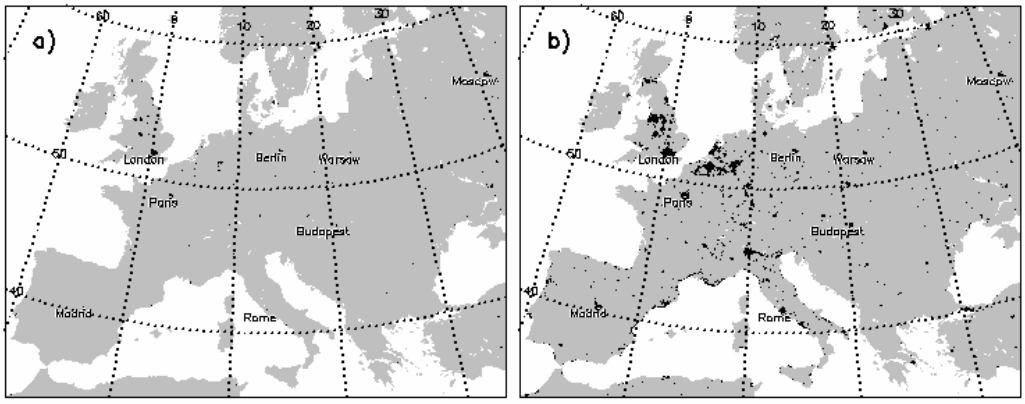

Figure 5. The standard GLCC-USGS urban land cover (a) and the new urban mask (b) at the spatial resolution of 10km. Urban areas are shown in black. The new map was derived at the spatial resolution of 1km by overlapping five different urban masks: GLCC-USGS, GLC2000, MODIS, LandScan, and DMSP.

The GLCC and GLC2000 underestimate total urban area in Europe (omission errors) while individual pixels that are mapped as urban in these data sets generally agree with the CORINE map and can be assumed to be correct. Urban areas in the MODIS land cover product occupy roughly the same total area as in CORINE, but large cities are mapped larger than they appear in CORINE (i.e. they are falsely classified as urban; commission errors). A general problem that appears across all these 1 km land cover classifications is that small towns and villages are mapped too small or are absent.

To produce a better map of urban areas at the spatial resolution of 1 km a simple method that makes use of the idea of 'convergence of evidence' is used. Five urban masks from different sources were overlaid and the agreement of at least two layers was used to map urban areas. Beyond the existing land use classifications GLCC, GLC2000, and the MODIS land cover product, urban masks were derived from the LANDSCAN population data set from the Oak Ridge National Laboratory (ORNL) as well as from the night light emissions recorded by the Defence Meteorological Satellite Program (DMSP). The latter has previously been used to map urban areas from space (Elvidge et al., 1999; Elvidge et al., 1997; Imhoff et al., 1997). These two

[9] Global LandCover 2000, Joint Research Centre from European Commission Directorate General
[10] Moderate Resolution Imaging Spectroradiometer Land Cover Types map from National Aeronautic and Space Administration

additional urban maps were produced by applying a threshold above which a pixel is considered to be urban. The thresholds were derived by statistical comparison of the continuous data fields from LANDSCAN and DMSP with CORINE. The thresholds (32 for DMSP and 360 for LandScan) were chosen where the agreement with the CORINE urban class was highest.

The newly derived urban mask (Figure 5b) appears to be of enhanced quality in comparison to existing classifications. However, it underestimates the urban area of Europe by ~10 % - while large cities are mapped slightly too large, this effect is overcompensated by small villages that are not present in the mask. The new urban mask is used in the model scenario for the present climate (URB). For more details on the new urban mask e.g. total urban and land areas see Appendix 5.

2.2.4. Modelling Protocol

To isolate effects of urbanization on the climate model simulations are performed according to two scenarios, which correspond to different states of urbanization. The NOU scenario represents a hypothetical situation with no urban areas and is defined as the baseline scenario. The URB scenario represents the climate in the presence of urban areas using the URB land cover map as model input.

The model domain for this study is centred at 50°N 15°E with the grid size of 10 km and it covers most of Europe (Figure 5). It is nested in an intermediate domain with 30 km spatial resolution (not shown) to avoid direct influences from coarse resolution boundary conditions. The model is driven at lateral boundaries of the intermediate domain by the one-degree resolution Final Analysis NCEP data from 2000-2005. The forcing at the lateral boundaries is applied every 12 hours, at 00:00 and 12:00 of each simulated day. An additional boundary condition needed for UCM, the inner temperature of buildings, is set to the constant 20°C for all simulations.

The model runs are restricted to periods when significant effects of urban areas on the climate can be expected, given the large computational costs of simulations. Previous investigations revealed that the strongest UHI – one of the major urban perturbations of the environment – occurs in winter (Montavez et al., 2000) and in summer (Bottyan et al., 2005; Unger et al., 2001). Thus, January and July of each year from 2000-2005 were chosen for simulations. The model is run for one-month

periods: each simulation starts in the beginning of the month and ends in the end of the month. Model output is written for every 3 hours.

The six years (2000-2005) for model initialisation at lateral boundaries were chosen according to the following criteria: 1) the data set should be representative for long term climate averages for Europe, 2) to provide all necessary data fields for the model initialisation, and 3) to have a fine spatial resolution. Chosen Final Analysis NCEP data set has an advantage of the fine spatial resolution (1 degree) as compared to other available datasets (2.5 degree, NCEP Reanalysis); however, it begins in late 1999 while Reanalysis datasets typically cover the second half of 20th century. To proof that the chosen period is representative for average climate in Europe, the average daily temperature ($T_{2000\text{-}2005}$) and daily precipitation ($PR_{2000\text{-}2005}$) are calculated over the 2000-2005 period and compared compare to the temperature ($T_{1980\text{-}2005}$) and precipitation ($PR_{1980\text{-}2005}$) calculated over the 1980-2005 period using the mentioned above NCEP Reanalysis dataset. The comparison reveals no significant differences between values of compared variables: $T_{1980\text{-}2005}$=19.2±0.9°C vs. $T_{2000\text{-}2005}$=19.4±0.8°C for July and $T_{1980\text{-}2005}$=0.1±1.6°C vs. $T_{2000\text{-}2005}$=0.0±1.1°C for January; $PR_{1980\text{-}2005}$=2.81±0.63 mm day^{-1} vs. $PR_{2000\text{-}2005}$=2.94±0.33 mm day^{-1} for July and $PR_{1980\text{-}2005}$=1.51±0.38 mm day^{-1} vs. $PR_{2000\text{-}2005}$=1.54±0.35 mm day^{-1} for January. The chosen Final Analysis NCEP dataset for 2000-2005 contains all data fields necessary for the model initialisation, has fine spatial resolution of 1 degree and is representative for the longer scale climate of 1980-2005. The combination of these characteristics makes the dataset a fair choice.

2.2.5. Analysis of simulations

The adequacy of the model is evaluated by comparing simulated (URB scenario) and measured near surface temperature and UHI for several sites. Observations of the near-surface (2 m above ground) temperature and/or of the difference in the temperatures between urban land and its rural surrounding e.g. UHI are extracted for eight cities from available literature (Alonso et al., 2003; Hupfer and Chmielewski, 1990; Klysik and Fortuniak, 1999; Montavez et al., 2000; Müller, 1983; Unger et al., 2001) and other publicly available sources of information (University of Basel[11],

[11] www.unibas.ch

WetterOnline GmbH[12], Urban Climate Homepage[13]). For the comparison with model output on the 10 km grid, only observations which represent thermal regime of a region of 0.5-10 km (whole city or a large part of it) are used. Observations on the local scale (0.01-0.10 km) are not taken into the analysis.

Effects of urban land use are detected via significance tests of the differences in temperature and precipitation between URB and NOU model scenarios. The analysis is performed for each grid point of the model domain separately (no spatial autocorrelation analysed). Time series which correspond to January and July are analysed separately in order to detect seasonal differences in urban land use effects. Before the significance test is applied, the interannual variability term is subtracted from the analysed timeseries. For the model output time series x of the month im the mean $\overline{x_{im}} = \sum_{id=1}^{30} x_{id}$ is subtracted from each element id (day) of x: $x'_{id} = x_{id} - \overline{x_{im}}$, id = 1,..30. Therefore, data series x' of different years can be processed in the statistical significance test at once as the time series of concatenated $\{x'_{2000}, x'_{2001}, x'_{2002}, x'_{2003}, x'_{2004}, x'_{2005}\}$. This data transformation allows analysis of seasonal temperature and precipitation changes in absence of interannual signal. Because this study focuses on urbanization-driven climate changes on the regional scale rather than on feedbacks between urban environments and the global climate change, suggested simulated period of six years is considered sufficient to perform accurate statistical analysis of the simulated effects. The statistical variations of the estimated effects are based on the time series of the daily differences between the URB and NOU model output.

Different significance tests were chosen for the temperature and precipitation time series due to the different character of the analysed data. The temperature differences are highly localized and the statistical filter Manns-Whitney-U-Test is applied to time series of diurnal temperature range, maximum and minimum temperatures. The precipitation data have high variance in time and space, so a variance-insensitive significance test is needed. The test should be rather sensitive to the sign of precipitation differences in order to detect a reduction or an increase. The Sign-test is used for time series of daily total precipitation. For both tests, the confidence level is

[12] www.wetteronline.de
[13] www.stadtklima.de

set to 0.05 and data values of every second day are taken into the statistical analysis to reduce autocorrelation of the data.

To characterize the spatial expansion of the urban climate anomalies a new quantitative parameter Regional Effect Index (*REI*) is introduced. *REI* is calculated as the ratio of the total area of affected land to the total area of urban land:

$$REI(x) = \frac{A_{aff\_rur}(x) + A_{urb}}{A_{urb}},$$

where x is one of the following variables: maximum diurnal temperature difference ($Tmax_{URB\text{-}NOU}$), minimum diurnal temperature difference ($Tmin_{URB\text{-}NOU}$), diurnal temperature range difference ($DTR_{URB\text{-}NOU}$), or precipitation difference ($PR_{URB\text{-}NOU}$);

$A_{aff\_rur}(x)$ – total area beyond cities where the differences of x are found;

A_{URB} – total area of urban land;

From the definition of *REI(x)* it is always greater or equal to 1.0 assuming that the urban land is always affected. If $A_{aff\_rur}(x) \rightarrow 0$ then $REI(x) \rightarrow 1$ and there is no regional effect. If *REI(x)* is significantly greater than 1.0 the changes of x are regional in character. The significance threshold was set to 0.025 (2.5 %) what means if $REI(x) > 1.025$ then there is a significant regional effect with respect to the variable x.

An additional statistical analysis is performed in order to find possible dependencies of the magnitude of urban effects and climate conditions of the region where these effects are found. For each urban pixel (*upix*), the average monthly temperature ($T_{nou,upix}$) and precipitation ($PR_{nou,upix}$) are calculated for January and July over six simulated years (2000-2005) from the NOU model simulation. Then the effects $Tmin_{URB\text{-}NOU,upix}$, $Tmax_{URB\text{-}NOU,upix}$, $DTR_{URB\text{-}NOU,upix}$ extracted for each pixel *upix*, are correlated to the $T_{nou,upix}$ and $PRC_{nou,upix}$. The correlation coefficients are then analysed for all *upix*s.

2.3. Results and Discussion

2.3.1. Corroboration of model results

Model simulations of the URB scenario are compared to available observations at several urban sites (Table 4) for near surface temperature and urban heat island. The UHI is calculated as the difference between near-surface temperatures at urban and rural sites. Observed and measured near-surface temperatures are averaged to the

same time step of 1 month, because the model temporal resolution (output every 3 hours) can represent the main temperature trend, but not fine-scale oscillations.

Modelled temperatures at Berlin, Madrid, and Salamanca agree well with observations in both seasons. The modelled UHI at Szeged, Lodz, and Granada are favourably compared to the measurements in both simulated seasons, while at Basel only the summer season simulations agreed well with the measurements of the near-surface temperature and UHI.

Table 4. Comparison of predicted near-surface temperatures and UHI (URB scenario) to available measurements at selected sites. Table cells marked by grey colour indicate a mismatch by more than 2°C between modelled and observed data.

Site name	Time		Near-surface temperature (°C)		Average UHI (°C)		Max. UHI (°C)	
			mod.	obs.	mod.	obs.	mod.	obs.
Szeged, Hungary	99 – 00	Jan	4.1	-1.1			1.5	1.4
		Jul	23.1	22.1			2.7	2.6
Lodz, Hungary	92 – 94	Jan						
		Jul	18.5	18.4			1.8	2.0
Granada, Spain	01 – 90	Jan	12.3	6.4	2.1	2.5	2.5	3.0
		Jul	28.3	25.7	4.3	1.8	4.6	3.6
Salamanca, Spain	96 – 98	Jan	6.3	5.3	1.1	2.3		
		Jul	22.5	20.9	1.8	2.7		
Basel, Switzerland	–	Jan	5.0	2.2			3.1	-2.0
		Jul	18.9	19.9			3.8	3.0
Moscow, Russia	–	Jan	-4.8	-9.9				
		Jul	18.3	19.0				
Berlin, Germany	09 – 99	Jan	1.2	-0.4				
		Jul	16.8	17.9				
Madrid, Spain	–	Jan	6.5	4.9				
		Jul	23.3	24.2				

The mismatch between modelled and measured near-surface temperatures in January at Basel and Granada can be explained by the poor representation of the terrain complexities within the model at the chosen spatial resolution. The temperature mismatch at Moscow and Szeged can be explained by the underestimated snow cover: the predicted snow cover height in Moscow is 13.4±11.4 cm against observed 24.6±6.2 cm; in Szeged it is 1.1±3.2 cm predicted against 4.6±9.3 cm observed. The lower value of simulated average snow cover height results from a larger number of snow-free days simulated versus observed and, thus, leading to a larger number of days when the albedo of the urban surfaces is low (due to dark colours of roads and roofs) and surface temperatures rise.

2.3.2. Effects of urban land cover on near-surface temperature

The transformation of vegetated land to urban land results in significant differences of near-surface temperatures (Figure 6). The effects during wintertime are local in character – only little territory of non-urban land is affected (*REI* is close to 1, Table 5). During summertime, the *REI* is larger, which indicates a stronger regional character of the effect: the maximum temperature and diurnal temperature range differences affect about 1/3 (28% and 37%) larger area than the total urban area (Table 5).

Table 5. Regional Effect Index (*REI*) for near-surface temperature differences. Differences with strong regional character are highlighted in bold.

Variable	REI in January	REI in July
$Tmax_{URB\text{-}NOU}$	1.01	**1.28**
$Tmin_{URB\text{-}NOU}$	1.00	1.06
$DTR_{URB\text{-}NOU}$	1.01	**1.37**

The diurnal temperature range (*DTR*) is strongly affected by the presence of urban areas (Figure 6a,b). The land use modification leads to a reduction of the *DTR* over the total land area of the model domain by −0.02±0.02°C in winter and −0.04±0.06°C in summertime. These numbers have a great uncertainty due to the strong spatial variation of the temperature differences.

The largest differences in temperatures are found in areas of land cover perturbation (urban land cover) where the average decrease of *DTR* accounts for −1.26±0.71°C in summertime and −0.73±0.54°C in wintertime. The strongest reduction of *DTR* occurs in cities that are situated in warm dry climates like Madrid, Barcelona, Milan, Rome, Marseille and sometimes reaches −4°C in summertime. In summertime, a significant reduction of *DTR* is also found beyond urban land; it accounts for −0.39±0.39°C but it never exceeds −1.50°C.

The *DTR* reduction results from changes of minimum and maximum diurnal temperatures. The average increase of the minimum diurnal temperature (*Tmin*) over all urban sites accounts for +1.53±0.49°C in summer and for +1.24±0.78°C in winter

while differences in the maximum diurnal temperature (*Tmax*) show strong spatial variation. These differences of minimum and maximum diurnal temperatures are attributed to changes in the geometrical and thermal properties of the perturbed areas as well as their energy balance.

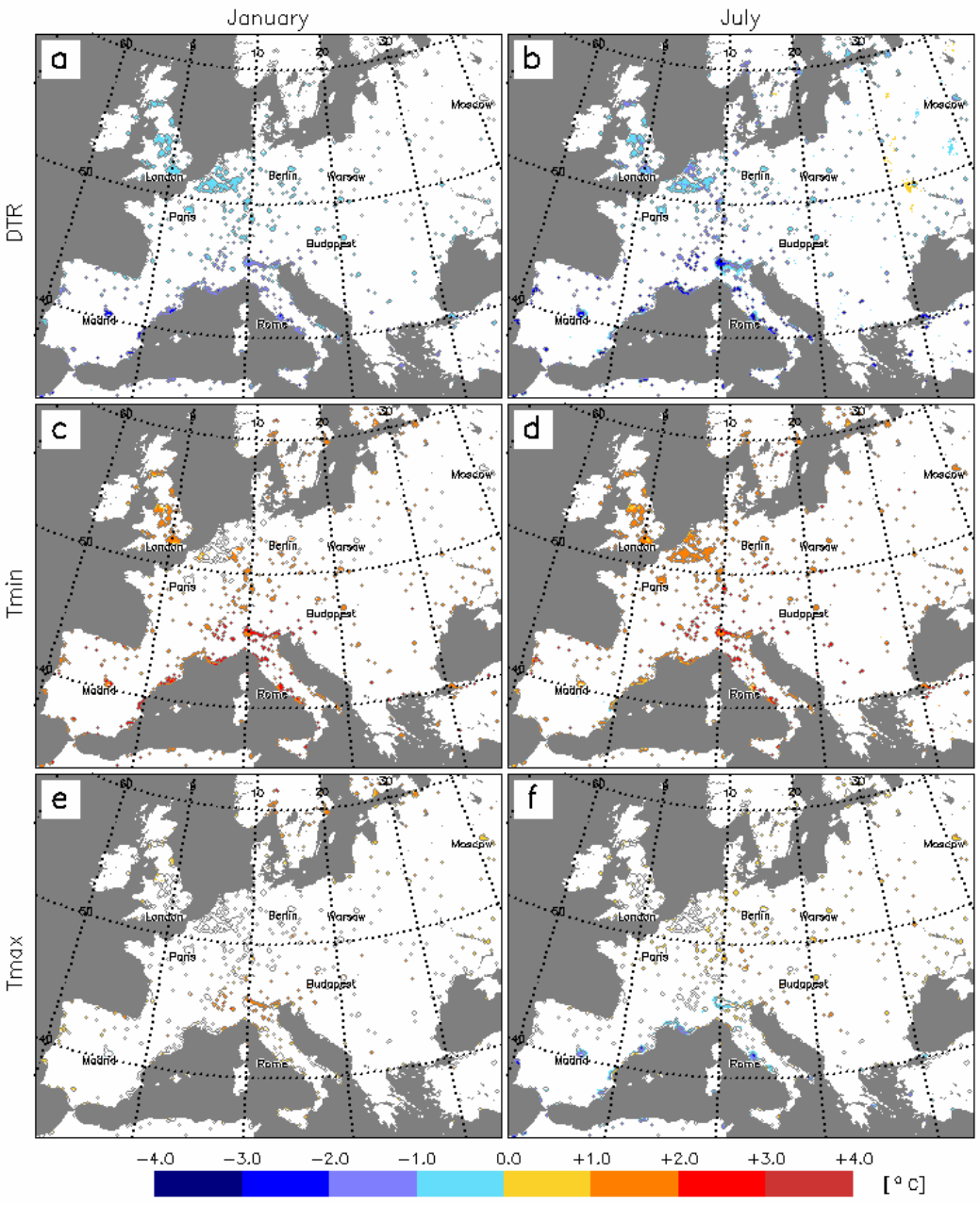

Figure 6. Effects of urban land cover on near surface temperatures (°C): (a) and (b) difference in diurnal temperature range ($DTR_{URB-NOU}$), (c) and (d) difference in minimum diurnal temperature ($Tmin_{URB-NOU}$), (e) and (f) difference in maximum diurnal temperature ($Tmax_{URB-NOU}$). Coloured areas identify places of statistically significant differences between URB and NOU model simulations.

The increase of *Tmin* has several reasons. In combination with lower albedo of urban surfaces (0.08-0.25), which cause larger energy absorption during day, the limited availability of surface water prevents evaporative cooling of urban areas and offsets the surface-to-atmosphere heat release thereby extending it to the night and early morning hours. During the night time the latent heat flux in urban areas is lower than in the rural areas (Figure 7c,d) due to the limited water availability for evapotranspiration, while the anthropogenic sources of sensible heat persist and contribute to the higher night sensible heat release (Figure 7a,b) as they are included in UCM. The reduced evapotranspiration in combination with the additional anthropogenic heat flux lead to an increase in near surface temperatures in urban areas – the effect also known as urban heat island (Figure 6c,d).

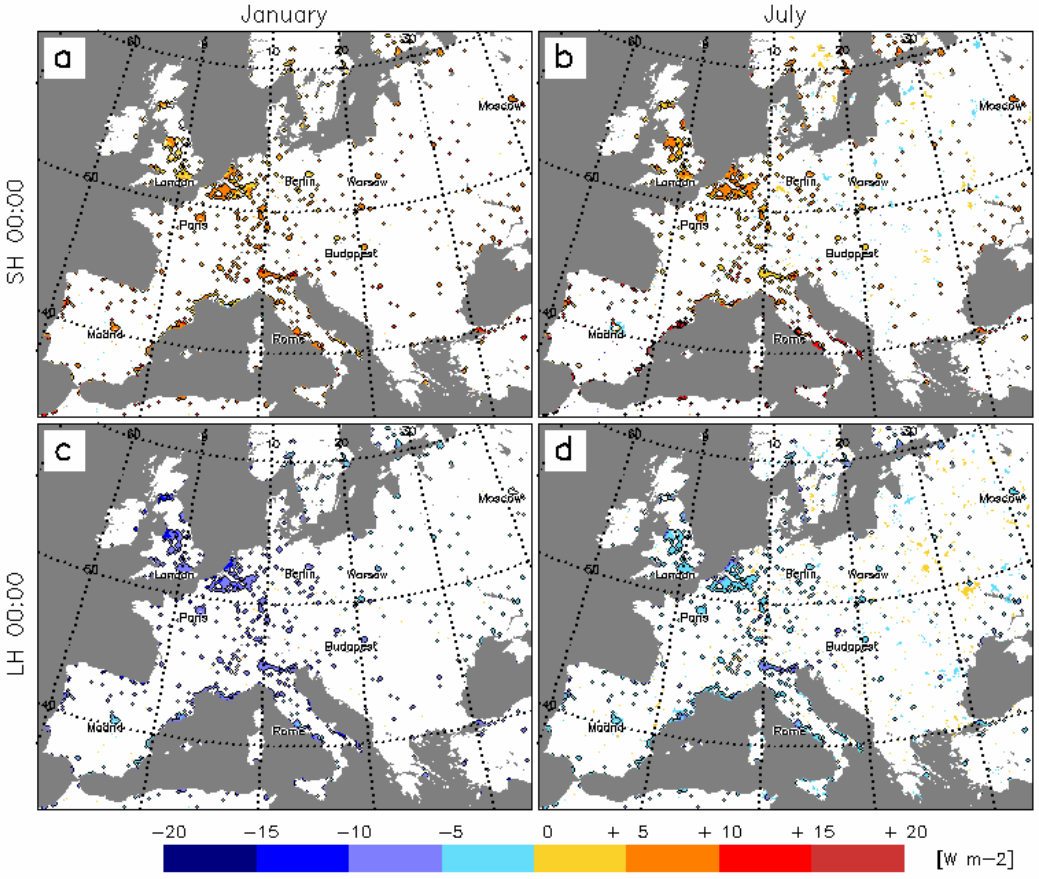

Figure 7. Effects of urban land cover on surface energy fluxes (W m^{-2}) at night hour 00:00: (a) and (b) difference in sensible heat flux ($SH_{URB-NOU}$); (c) and (d) differences in latent heat flux ($LH_{URB-NOU}$). Coloured areas identify places of statistically significant differences between URB and NOU model simulations.

Differences in *Tmax* indicate a reduction in Southern Europe by −0.87±0.39°C in summer and by −0.79±0.18°C (Figure 6e,f) while, in regions with temperate climate, *Tmax* is increased by +0.83±0.21°C and +1.03±0.35°C in summer and in winter respectively (Figure 6e,f).

In high latitudes during wintertime, agricultural land or grassland may be covered by snow while buildings protrude above the snow cover and expose wall surfaces to the atmosphere. Walls of buildings usually have darker colour than snow - this reduces albedo of the urban area and causes absorption and accumulation of a larger amount of the incoming solar radiation. Impervious materials usually have a larger heat storage capacity. Furthermore, buildings are heated to support a constant temperature inside. In wintertime, the outer atmosphere usually has a lower temperature and that causes a heat release from the buildings to the atmosphere. These factors in combination with the drag force induced by buildings on the air flow, which leads to the loss of momentum, result in an increase of near-surface temperature in wintertime simulations for high latitudes cities.

In summer time, an opposite effect might occur: *Tmax* in urban areas is lower than *Tmax* in rural surroundings (Figure 6f, urban areas of Southern Europe). There are several reasons for this: 1) hysteresis of the urban canopy system; 2) the lower inner building temperature as compared to the air temperature outside buildings; 3) partial shading of urban surfaces (roads, walls) due to presence of buildings and small sky view factor. To illustrate this situation the Figure 8 shows an offset in the phase of the diurnal temperature variation between the urban and the rural surfaces: the urban temperature reaches its highest value by ~3 hours later than the temperature at the rural place; the amplitude of temperature diurnal variation in urban areas is smaller than in rural area. The ground flux in the urban area is higher than in the corresponding rural area – a combined effect of low urban albedo and low canyon winds. Another important feature to see on the Figure 8 is that the ground flux integrated over 24 hours in this case might be offset from the 0-level due to the additional input of anthropogenic heat sources (sensible heat flux).

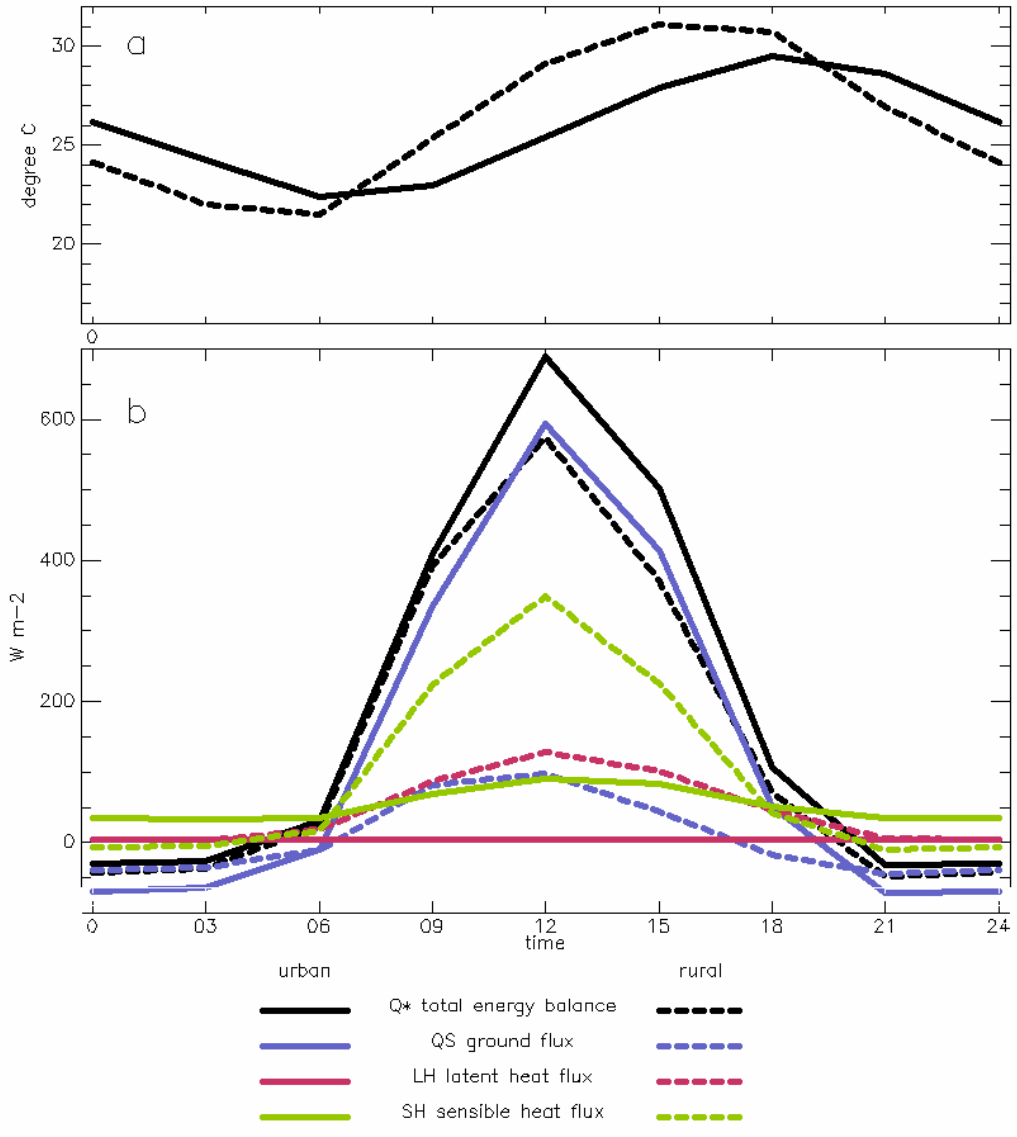

Figure 8. The near-surface temperature (a) and energy balance (b) of urban and rural surfaces. The data are 30-days averages over model simulations for Madrid.

In attempt to find a dependence of the described effects on the climate conditions of the regions where the effects occur, the linear regression analysis is performed for the time series of $DTR_{URB\text{-}NOU}$, $Tmax_{URB\text{-}NOU}$ *and* $Tmin_{URB\text{-}NOU}$ and the average climate variables (temperature and precipitation). The strongest correlation (correlation coefficient >0.50) are found between $Tmax_{URB\text{-}NOU}$ and the average daily temperature in January and July, for $Tmax_{URB\text{-}NOU}$ and average precipitation in July (Table 6). The interpretation for these correlations: a stronger increase of *Tmax* occurs in colder regions (cooler temperate climates) in both seasons, and an increase of *Tmax* in July is more likely to happen in regions with higher precipitation (cooler temperate climates).

Table 6. Correlation coefficients between the strength of urban effects on $Tmin_{URB-NOU}$, $Tmax_{URB-NOU}$, or $DTR_{URB-NOU}$ and the average temperature (T_{NOU}) and precipitation (PR_{NOU}) of the background simulation (NOU scenario). The three largest correlation coefficients are highlighted in bold.

Correlated variables	January	July
T_{NOU}, $Tmin_{URB-NOU}$	0.20	-0.12
PR_{NOU}, $Tmin_{URB-NOU}$	-0.06	0.14
T_{NOU}, $Tmax_{URB-NOU}$	**-0.55**	**-0.60**
PR_{NOU}, $Tmax_{URB-NOU}$	0.00	**0.60**
T_{NOU}, $DTR_{URB-NOU}$	-0.43	-0.14
PR_{NOU}, $DTR_{URB-NOU}$	0.30	0.23

2.3.3. Effects of urban land cover on precipitation

Our simulations show that differences in daily precipitation between NOU and URB scenarios are highly variable over the whole domain (Figure 9). Induced by the presence of urban land, significant differences in precipitation ($PR_{URB-NOU}$) spread out far beyond urban areas and affect large rural surroundings providing high *REI* (6.4 in winter and 5.8 in summertime).

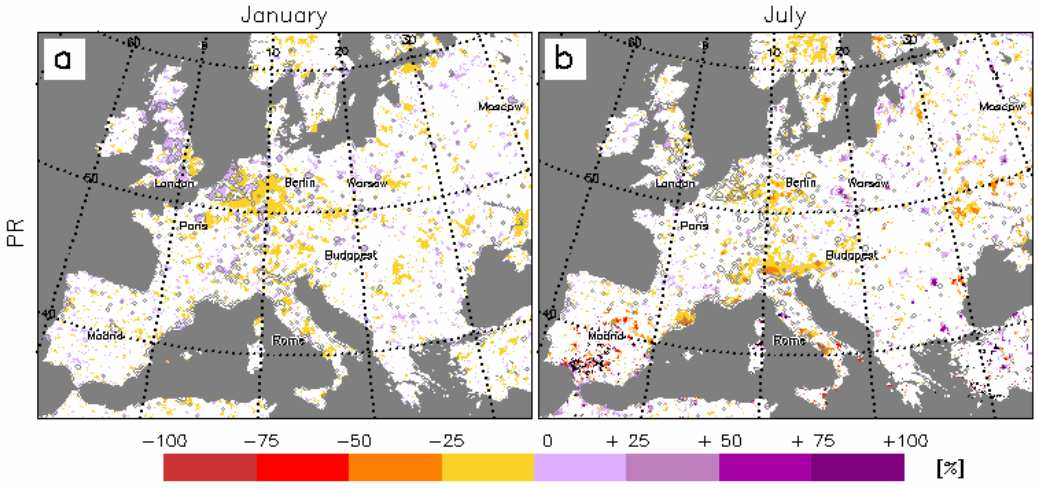

Figure 9. Effects of urban land cover on the daily precipitation (%). The relative to the baseline daily precipitation differences $PR_{URB-NOU}$ / PR_{NOU} (%) are shown in colour for January (a) and July (b) simulations.

Due to the extensive land area included into the model domain, which comprises areas with different climates and, thus, different monthly precipitation rates, $PR_{URB-NOU}$ is analysed in relation to the background monthly precipitation (PR_{NOU}):

$\Delta PR_{URB-NOU} = 100\ PR_{URB-NOU} / PR_{NOU}$

In winter, the average $PR_{URB-NOU}$ over land of the whole domain is as low as −0.00±0.06 mm day^{-1} (−0.07±0.02 mm month^{-1}). The precipitation differences are mostly found over urban areas and downwind from urban areas, not upwind. The average $PR_{URB-NOU}$ over urban land ($UPR_{URB-NOU}$) and over rural land ($RPR_{URB-NOU}$) show opposite trends accounting for +0.09±0.16 mm day^{-1} and −0.04±0.14 mm day^{-1} respectively. The positive $UPR_{URB-NOU}$ accounts for +0.21±0.14 mm day^{-1}, what makes for $\Delta UPR_{URB-NOU}$ = +8±4 % of the background value calculated from the *NOU* scenario (UPR_{NOU}). As it can be seen from the Figure 9a, the small cities tend to produce an increased rainfall downwind of the city (the dominant winds are westerly), while large urban areas produce an increased rainfall over the city. This locality can be partly explained by the scheme for the cumulus parameterisation chosen for the model setup. The precipitation increase over urban areas results form the enhanced convection forced by UHI: higher surface temperatures provide an increase in the moist static energy of cloud and result in an increase of cloud water mixing ratio; when the saturation value is reached, the precipitation is initiated. Chosen for the simulations cumulus parameterization includes no liquid cloud water and thus, rainfall occurs as soon as the precipitation formed. After the rainfall over an urban area the air mass becomes less saturated ("dry") and moves downwind. This urban intensified precipitation pattern results in reduced rural precipitation ($RPR_{URB-NOU}$) by −0.12±0.11mm day^{-1}, what is −4±3 % of the background value RPR_{NOU}. Possible dislocation of simulated precipitation patterns due to the model setup are considered of minor importance for the performed analysis since this study is not focused on locating precipitation anomalies exactly, but rather on giving a quantitative estimation of urbanization-induced precipitation changes over a long period of time.

In summer, the average $PR_{URB-NOU}$ over land of the whole domain is −0.03±0.25 mm day^{-1} (−1.05±1.31 mm month^{-1}). The precipitation differences are highly variable over the domain and can be classified in three groups by geographical location. Multiple urban areas situated in coastal regions and inland between 15°E and 30°E (EAST_EU) exhibit enhanced rainfall (Figure 9b) in urban areas ($UPR_{URB-NOU}$ = +0.18±0.19 mm day^{-1}). Urban areas between 10°W-15°E and 45°N-55°N

(CENTRE_EU) as well as urban areas between 10°W-15°E and 35°N-45°N (SOUTH_EU) mainly produce reduced rainfall over cities by $UPR_{URB\text{-}NOU}$ = –0.41±0.35 mm day^{-1}), which is lower than UPR_{NOU} by –19±15 %. In rural areas in CENTRE_EU and SOUTH_EU regions, significant values of $RPR_{URB\text{-}NOU}$ are found mainly in south-east of urban areas (downwind) and account for –0.55±0.52 mm day^{-1} ($\Delta RPR_{URB\text{-}NOU}$ = –18±15 %).

The differences in effects on precipitation among EAST_EU, CENTRE_EU and SOUTH_EU regions might be explained by differences in climate of these regions. The region SOUTH_EU has Mediterranean climate with dry and hot summers (Cfb climate class according to Köppen's climate classification) while CENTRE_EU has and Maritime West Coast climates (Csa, Csb) and EAST_EU region is largely influenced by Humid Continental climate (Dfb). In SOUTH_EU the air humidity during dry hot (clear-sky conditions) summers is low in urban areas an additional removal of water into the surface runoff cuts off the contribution of the surface evaporation to the precipitation formation (Appendix 3 shows the water loss into the surface runoff and the underground runoff). The values of relative precipitation change $\Delta PR_{URB\text{-}NOU}$ in SOUTH_EU reach up to 30 % reduction because the background value PR_{NOU} is small. In EAST_EU region, summers are humid and thus, urban heating forces the convection and precipitation formation (similar to the situation described above for the winter simulations). In CENTER_EU region summers are generally mild and precipitation is frequent, so that the reduction of the precipitation can be explained by the reduced surface water availability in the extensive urban areas of this region.

Various measurement studies report an increase of precipitation in urban areas and downwind of urban areas (Changnon Jr. et al., 1991; Huff and Changnon Jr., 1973; Jauregui, 1991; Shepherd et al., 2002). However, it is difficult to compare the results of this study to the observations for two reasons: 1) most reported observations of precipitation are done within the tropical region between 32°N-32°S (Changnon Jr. et al., 1991; Rosenfeld, 2000; Shepherd et al., 2002) where the domain of the present study is not included; 2) these studies compare the rainfall downwind of a city to the rainfall upwind of the city, while in this work rainfalls simulated with and without urban areas are compared. The latter argument is important for the correct interpretation of the results: this study gives an estimation of a contribution of urban land cover to precipitation (and near surface temperatures), not modifications of

precipitation patterns by existing urban areas; here two simulated states of atmospheric circulation are compared, while observational studies analyse only one that is influenced by urban surfaces.

The analysis of dependence between $PR_{URB\text{-}NOU}$ and climate condition (average monthly temperature and precipitation amount) do not show any significant correlation (correlation coefficients are always less than 0.02) for either of the regions.

The combination of both effects, i.e. increased near-surface temperature and reduced air moisture, causes expansion of the lower atmosphere and an increase in surface pressure, which is found in highly urbanized areas (see Appendix 4).

2.4. Summary and outlook

This study has suggested that urban land cover significantly alters near-surface temperatures and precipitation at local and regional scales. It was found that locally (in places of land cover change) a significant reduction of the diurnal temperature range by more than −1.2°C in summertime and more than −0.7°C in wintertime, an increase of ~8% in winter precipitation and a reduction of ~19% in summer precipitation can be attributed to the transformation from vegetated to urban land. It was shown that the effects of urban land cover are regional in character: not only the local climate of perturbed areas but also the one of surrounding land is affected. This result is especially important for predicting impacts of urban growth on local and regional climate.

However, two major factors were not included into this study: 1) effects of urban pollution on precipitation formation processes as described in the work of Rosenfeld (2000) ; 2) no differential representation of morphology and anthropogenic heat sources for each individual city. The latter issue shows a necessity for development of a new database which will contain standardised information about development and structure of multiple individual cities.

Results of this study revealed significant effects on the local and regional climate caused by urbanization at its present state and encourage for a future research on the urbanization as a dynamic process. A study on estimating possible climate responses to the growth of urban areas would require precise urban mapping with short time intervals (3-5 years) to represent the dynamics of urban development. The database

of urban maps would have to satisfy strict requirements on the uncertainty of the land cover mapping at high spatial resolution.

Effects of urban air pollution on the climate were not addressed in this study although the contribution of urban air pollution to the climate is of great importance and might cause strong effects on the cities' surroundings, affecting the terrestrial biosphere. Studying these effects would require the use of additional components, e.g. terrestrial biosphere, atmospheric chemistry and transport for a future research.

3. Effects of urban areas expansion on precipitation and near-surface temperature in Europe

3.1. Introduction

Urban population is growing at a much faster rate than the Earth's population as a whole, and by larger annual increments than ever before. By the middle of 21st century most people in the world will live in urban areas. In most developing regions, the proportion of people living in the largest cities is also increasing, in contrast to Europe, where more than 40 % of the urban population live in small and middle size cities.

Given the future urbanization projections and estimations of impacts of individual cities on the environment, it becomes important to investigate effects of multiple growing urban areas. However, the way of urban growth remains uncertain: while small cities might experience some population densification, in large metropolitan areas an expansion of low populated suburban land occurs. For example, the average built-up area per person, defined simply as the reciprocal of the average density and measured in square meters per person, was 190 m^2 in 1990 and 230 m^2 in 2000 in cities of Europe (Cities Alliance[14]).

With the assumption that the population's average income and demands for space are not changing, the population densification in a city would lead to the construction of higher buildings, while in case of urban land expansion into suburban areas the structure of buildings and occupied spaces would remain constant. These processes, alone or in combination, lead to changes in cities' structure and size and might result in different impacts of urban land on the local and regional climate.

This chapter is focused on an estimation of potential urbanization impacts on the near-surface temperature and precipitation in Europe at local and regional scales. Two scenarios, which represent different strategies of urban growth, are analysed: 1) an increase of buildings' average height and 2) an expansion of urban sprawl into suburban land.

[14] www.citiesalliance.org

3.2. Materials and Methods

3.2.1. Regional model

The limited-area numerical weather prediction mesoscale PSU/NCAR model MM5 with UCM land surface scheme is used for simulations (see "1.2.1. Regional model MM5", on page 16). The model parameters are set to represent a typical middle-size European city (Table 3) as outlined in the chapter "2.2. Materials and Methods" on page 16.

The MM5-LSM-UCL model is used to estimate effects on near-surface temperatures and precipitation from potential states of urbanization, which result from two different strategies of urban growth.

3.2.2. Mapping urban areas

Three land cover maps were created to represent the following states of urbanization: 1) a land cover map that includes no urban area (NOU), 2) a land cover map with urban areas (URB), and 3) a land cover map that represents expanded urban areas (2URB). The 2URB map was designed to contain the total urban area twice as large as the total urban area in the URB urban mask. Thus, the 2URB map represents "doubled" urban area from the "real" urban area.

Several data sets were used in order to refine the spatial distribution of the cities. The NOU and the URB land cover maps were derived as described in the chapter "2.2.3. Mapping urban areas" on page 18.

The 2URB map was created using a proxy indicator (urban score) of urban area extent. To acquire the urban score map several available data sets were used: CORINE, GLCC-USGS, GLC2000, and the MODIS land cover databases (urban land cover classes) as well the LandScan population data set from the Oak Ridge National Laboratory (ORNL[15]) and night light emissions recorded by the Defence Meteorological Satellite Program (DMSP[16]). In contrast to the other databases, the DMSP and LandScan data have continuous data fields. To extract an urban mask for these datasets the setting of the appropriate thresholds is necessary. The thresholds were defined by minimizing the mismatch in urban class mapping between the

[15] www.ornl.gov/sci/landscan/
[16] http://msl.jpl.nasa.gov/Programs/dmsp.html

DMSP|LandScan and CORINE dataset. For more details on LANDSAT and DMSP based urban mask see "2.2.3. Mapping urban areas" on page 18.

The CORINE urban map (map with masked out urban land) has a spatial resolution of 250 m and was used as the reference urban map for the validation of the CLCC, CLC2000, MODIS, DMSP, and LandScan urban maps. Each of the individual urban maps (*imap*) was compared to CORINE and the accuracy of the urban class mapping was calculated as the number of pixels where CORINE and *imap* agree on urban land use category. The degree of the match between the urban mask of *imap* and the urban mask of CORINE (Table 7) was calculated as:

$$P(imap) = \frac{N_{urban}(imap)}{N_{total}(imap)},$$

where

$N_{urban}(imap)$ is number of urban pixels in both urban maps: *imap* and the reference map CORINE;

$N_{total}(imap)$ is number of urban pixels in *imap*;

imap = GLCC|GLC2000|MODIS|DMSP|LandScan;

Table 7. Probabilities *P* of urban mask match between each individual urban map *imap* and the reference urban map CORINE.

Names of database from which the urban map was derived	*P*(*imap*)
GLCC-USGS	57 %
GLC2000	47 %
MODIS	29 %
LandScan	0 – 68 %, dep. on threshold value
DMSP	0 – 72 %, dep. on threshold value

From the definition: if the urban masks in *imap* and CORINE match, the *P(imap)*=1, otherwise *P(imap)*<1. For each pixel in *imap* in the row *i* and column *j*, $P_{i,j}(imap)=P(imap)$. The *P*(*imap*) can be interpreted as a probability of *imap* urban mask to match the urban mask in the reference dataset CORINE.

The urban score map (USM) was calculated as the sum of all of individual probability urban maps *P*(*imap*):

$USM_{i,j} = \sum_{imap} P_{i,j}(imap)$, for each *i*=0,..*nr*-1 and *j*=0,..*nc*-1,

where

imap = GLCC-USGS|GLC2000|MODIS|DMSP|LandScan;

nr and *nc* are numbers of rows in and columns in *imap*;

From this definition, the maximum value is USM is 5 and this means that all individual maps agree, while the minimum value is 0 means that none of individual maps matches the other on urban land mask.

The reference urban map (URB), which represents 100 % urban areas in Europe, was derived from the USM by setting a threshold (*threshold_100%*), which masks urban areas as close as possible to the CORINE database. The optimal threshold was calculated by minimisation of the mismatch of urban masks between USM and CORINE (where CORINE is defined):

$$\left|\text{UrbanArea}\left(\text{USM}\left(threshold\_100\%\right)\right) - \text{UrbanArea}\left(\text{CORINE}\right)\right| \to 0$$

Therefore, the 100% urban area reference map (URB) is defined as:

$$\text{URB} = \text{USM}\left(threshold\_100\%\right),\ threshold\_100\% = 0.56$$

In order to create the 2URB map, an appropriate threshold (*threshold_200%*), which defines the total urban area twice as large as in the URB map, was applied to USM. The threshold was calculated by minimizing the difference between the total urban area in USM and total urban area of USB multiplied with factor two:

$$\left|\text{UrbanArea}\left(\text{USM}\left(threshold\_200\%\right)\right) - 2 * \text{UrbanArea}\left(\text{URB}\right)\right| \to 0$$

$$2\text{URB} = \text{USM}\left(threshold\_200\%\right),\ threshold\_200\% = 0.25$$

The 2URB map (Figure 10) has a twice as large total urban area as the URB map. However, the 2URB urban mask includes area which accounts for only ~180 % of CORINE total urban area. This effect is due to the fact that the CORINE database includes more small urban areas on the spatial resolution of 250 m, which are omitted on the resolution of 1km in the 2URB map. For more details, e.g. total urban and land areas see Appendix 5.

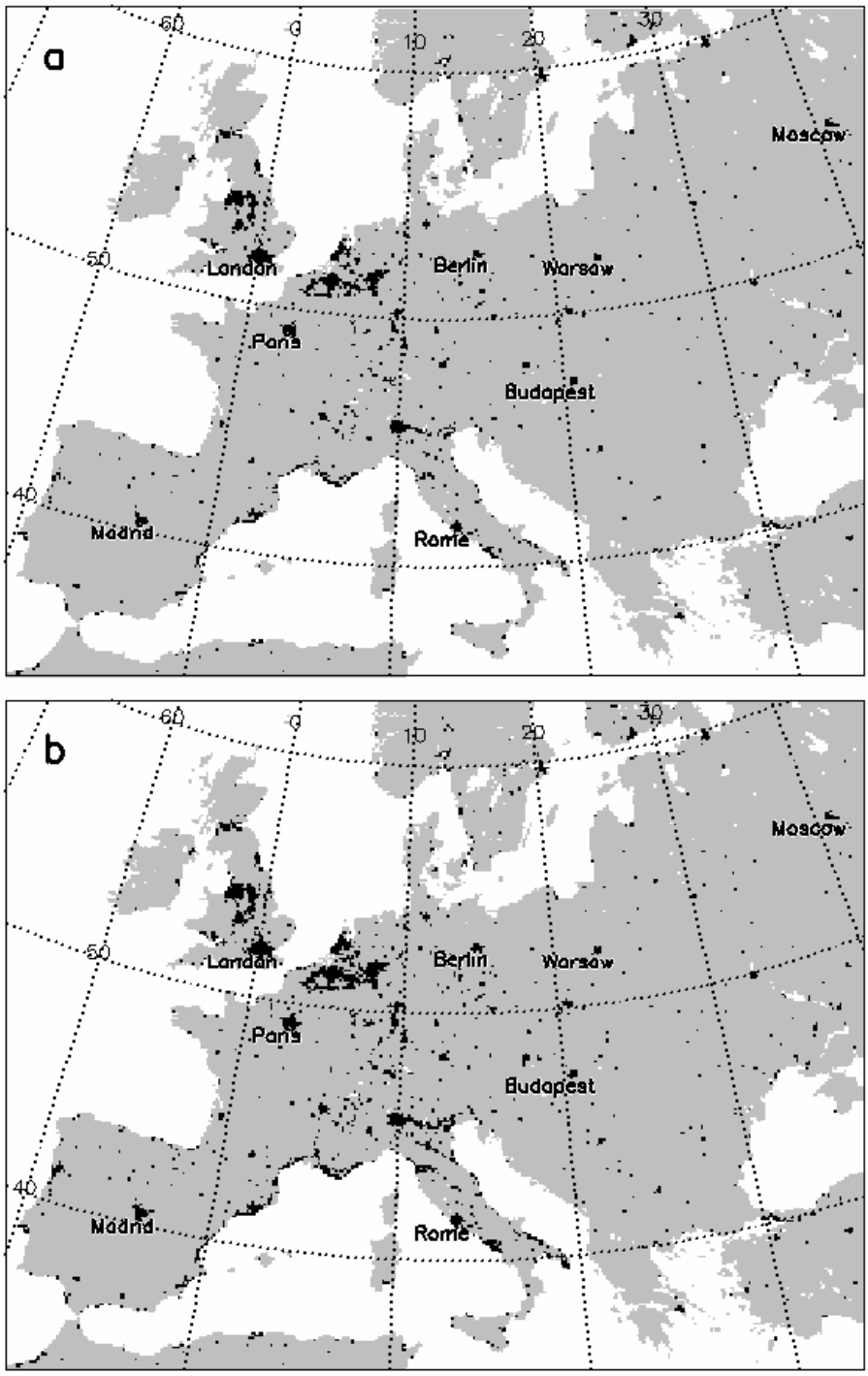

Figure 10. The present state urban mask (a) and the urban mask where urban areas occupy two times larger territory (b) at the spatial resolution of 10 km. Urban areas are shown in black.

3.2.3. Modelling Protocol

For the analysis of urban growth effects on the climate, model simulations are performed according to four scenarios (Table 8) which correspond to different states of urbanization and urban growth strategies. The NOU scenario represents a hypothetical situation with no urban area and is defined as the base-line scenario. The URB scenario represents the climate in presence of urban areas using the URB land cover map as the model input. This scenario corresponds to the "actual" state of urbanization in 2000-2005. Scenarios 1URB and 2URB represent urbanization states, which result from vertical and horizontal urban expansion strategies respectively. Within the 1URB scenario it is assumed that urban area boundaries do not change (remain as in the URB scenario) but the average building height increases with the factor two. According to the 2URB scenario, the average building height remains constant (as in the URB scenario), but the total urban area is twice as large as in the URB scenario.

Table 8. Model scenarios which represent different urban states and urban growth strategies.

Simulation	Description
NOU	Base-line scenario; no urban land present
URB	Scenario represents "actual" state of urbanization: single urban class is included into the land cover map
1URB	Vertical expansion - single urban class as in URB scenario, but the building height is doubled
2URB	Horizontal expansion - single urban class, the total urban area is twice as large as in URB scenario, the building height as in URB scenario

The configuration of the model setup is described in the chapter "2.2. Materials and Methods" on page 16.

3.2.4. Analysis of the simulations

Effects of urbanization on climate are detected via significance tests of the differences in temperature and precipitation for the following pairs of scenarios:

URB-NOU, 1URB-NOU, and 2URB-NOU. More details on the choice of the significance tests see in the chapter "2.2.5. Analysis of simulations" on page 21.

The Regional Effect Index (*REI*) is used to characterize the spatial expansion of the urban climate anomalies. It is calculated as the ratio of the total area of the affected land to the total area of the perturbed land as in "2.2.5. Analysis of simulations" on page 21.

Regional effects of urban growth on the near-surface temperature or precipitation are compared via *REI* indexes. If the difference between the *REI* indexes of two scenarios exceeds the significance threshold (0.025, which is 2.5% of [max*REI*=1]), the effects of the corresponding urbanization states on the regional climate are "significantly different" if:

$|REI(x,URB) - REI(x,urb)|>0.025$, e.g. urban land in the URB-scenario has a significantly different regional effect on x than the urban land in the scenario *urb*, where *urb* = 1URB|2URB.

3.3. Results and Discussion

3.3.1. Effects of urban growth on near-surface temperature

The replacement of vegetated land by urban land (NOU and URB scenarios) results in significant effects on near-surface temperature (see "2.3.2. Effects of urban land cover on near-surface temperature" on page 25).

The 1URB scenario, which corresponds to the vertical urban growth, provides similar spatial patterns and the magnitude of temperature differences between the base-line and the 1URB scenarios as between the base-line and the URB scenarios (Figure 11). The *REI* values for near-surface temperature differences provided by the 1URB and the URB are insignificantly different for both seasons (Table 9):

$|REI(x,\text{URB})-REI(x,\text{1URB})|<0.025$ for $x=Tmin|Tmax|DTR$;

According to the 1URB scenario, the effects on near-surface temperature in January are local in character, while *REI* in July is larger than 1.025, a fact that indicates the regional effect on the maximum daily temperature and diurnal temperature range (Table 9). Low temperatures and high moisture content in the air during cloudy days provide the local character of the temperature differences in winter: the city's warm air mass cools quickly once it emerges in the rural colder

atmosphere. The snow cover, which serves as a water reservoir, mitigates the urban warming, because urban and rural surfaces interact with the lower atmosphere through the "snow-buffer". In fact, due to the urban heat island the snow cover within a city often melts and evaporates cooling the surface.

Table 9. Regional Effect Index (*REI*) - ratio of the total area affected by the near-surface temperature differences to the total urban area. The vertical cities' expansion (scenario 1URB - doubling of building height) results in similar *REI* indexes to the present day scenario URB. Note: For URB and 1URB scenarios, urban area is the same while for 2URB scenario it is a twice-larger area.

Variable	*REI* in January	*REI* in July
$Tmax_{URB\text{-}NOU}$	1.01	**1.28**
$Tmax_{1URB\text{-}NOU}$	1.01	**1.29**
$Tmax_{2URB\text{-}NOU}$	**1.30**	**2.43**
$Tmin_{URB\text{-}NOU}$	1.00	1.06
$Tmin_{1URB\text{-}NOU}$	1.00	1.06
$Tmin_{2URB\text{-}NOU}$	**1.83**	**2.56**
$DTR_{URB\text{-}NOU}$	1.01	**1.37**
$DTR_{1URB\text{-}NOU}$	1.01	**1.38**
$DTR_{2URB\text{-}NOU}$	**1.95**	**2.68**

The 2URB, which scenario corresponds to the horizontal expansion of urban sprawl, and provides a significantly larger proportion (large *REI* values) of rural land affected by temperature differences as compared to the 1URB scenario (Table 9). Large differences between *REI*(x,2URB) *and* *REI*(x,1URB), where x=*Tmin*|*Tmax*|*DTR*, are found in simulations for July and January (Table 9). The *REI* values in summertime simulations reach more than 2.5. This means that a land area more than 2.5 times larger than the total urban area is affected by significant differences in temperatures ($X_{2URB\text{-}NOU}$). For instance, *REI* for $Tmin_{URB\text{-}NOU}$ is 1.06 and for $Tmin_{2URB\text{-}NOU}$ is 2.56. The total urban area in the URB scenario is S_{URB} = 159.1 km^2 and the total urban area in the 2URB scenario S_{2URB} = 222.8 km^2 (Appendix 5). The total affected by *Tmin* differences area is then in URB scenario: $STmin_{URB}$= 1.06 * 159.1 = 168.6 km^2 and in 2URB scenario $STmin_{2URB}$ = 2.56 * 222.8 = 570.4 km^2. The ratio between $STmin_{URB}$ and $STmin_{2URB}$ is then 1:3.4. That means the area, where *Tmin* is significantly affected by expanded cities, is 3.4 times larger than the area affected

by the cities today ("actual" state of urbanization relevant for 2000). In other words, the increase of urban area in proportion 1:2 leads to an expansion of affected area in proportion 1:3.4. This proportion suggests that the magnitude of urban effects on temperature might not be linear dependant on the size of cities.

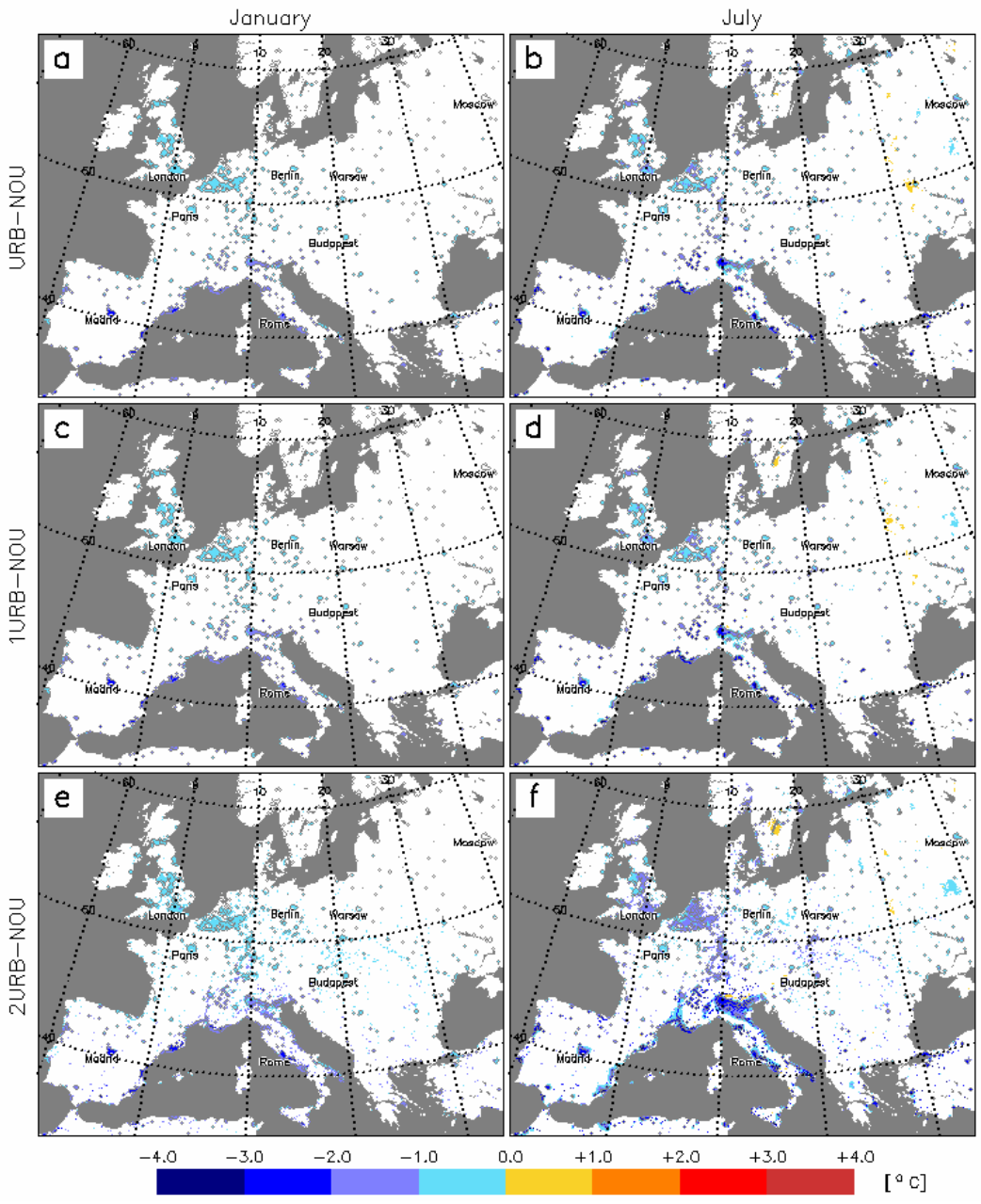

Figure 11. Differences in diurnal temperature range $DTR_{URB-NOU}$ ((a) and (b)), $DTR_{1URB-NOU}$ ((c) and (d)), $DTR_{2URB-NOU}$ ((e) and (f)).

The values of $x_{2URB-NOU}$, $x_{1URB-NOU}$, and $x_{URB-NOU}$ (x=*Tmin*|*Tmax*|*DTR*) are of the same order of magnitude for January and July (Table 10). In July all three urban scenarios (URB, 1URB, and 2URB) provide stronger increase of urban *Tmin* than in

January and thus result in a stronger reduction of *DTR*. The magnitude of this reduction is variable over the model domain with its maximum in urban areas of Southern Europe (Figure 11).

The 2URB scenario provides a larger proportion of rural land affected by temperature differences due to urban temperatures from enlarged cities and multiple villages. On the scale of this study (10 km) more urban areas appear in the 2URB mask because they are sufficiently large (after the expansion) to overcome the urban class threshold in the land use classification.

Table 10. Differences in near-surface temperatures (°C) between scenarios, which include urban land, and the base-line scenario. The "affected land" values are calculated over urban and rural land where a significant difference between two scenarios was found. The "urban land" values are calculated over urban land only. Note: For URB and 1URB scenarios, urban area is the same while for 2URB scenario it is a twice-large area.

Variable	January		July	
	affected land	urban land	affected land	urban land
$Tmax_{URB\text{-}NOU}$	+0.96±0.50	+0.30±0.50	−0.17±0.90	+0.09±0.61
$Tmax_{1URB\text{-}NOU}$	+0.93±0.53	+0.30±0.51	−0.22±0.89	+0.07±0.60
$Tmax_{2URB\text{-}NOU}$	+0.83±0.81	+0.21±0.48	−0.82±0.81	−0.27±0.77
$Tmin_{URB\text{-}NOU}$	+1.58±0.48	+1.24±0.78	+1.45±0.61	+1.53±0.49
$Tmin_{1URB\text{-}NOU}$	+1.58±0.49	+1.25±0.78	+1.43±0.62	+1.52±0.48
$Tmin_{2URB\text{-}NOU}$	+1.54±0.57	+1.13±0.80	+0.98±0.95	+1.22±0.58
$DTR_{URB\text{-}NOU}$	−0.88±0.47	−0.73±0.54	−1.05±0.74	−1.26±0.71
$DTR_{1URB\text{-}NOU}$	−0.88±0.47	−0.73±0.54	−1.04±0.74	−1.26±0.71
$DTR_{2URB\text{-}NOU}$	−0.93±0.48	−0.81±0.59	−1.32±0.81	−1.49±0.81

The small differences between the near-surface temperatures of the URB and the 1URB scenarios show that the doubling of buildings' height does not significantly change the thermal regimes in cities. However, the parameterisation of urban land might be the source of this insignificance because of the simplified energy balance for the walls. The land-surface model resolves the energy balance of the whole wall at once, while it neglects the energy fluxes within and along walls. However, including multiple layers into the model would increase computational cost and not necessarily capture the energy balance better (Kusaka and Kimura, 2004).

The reduction of *DTR* results from changes of minimum and maximum diurnal temperatures.

The minimum diurnal temperature increases due to the urban heat island (see chapter 1.3.2. Simulation of near-surface temperature by the standard MM5-LSM and MM5-UCM" on page 11) (Figure 12). The $Tmin_{1URB\text{-}NOU}$ is of the same effect as the $Tmin_{URB\text{-}NOU}$ while the $Tmin_{2URB\text{-}NOU}$ is slightly lower in both seasons (Table 10).

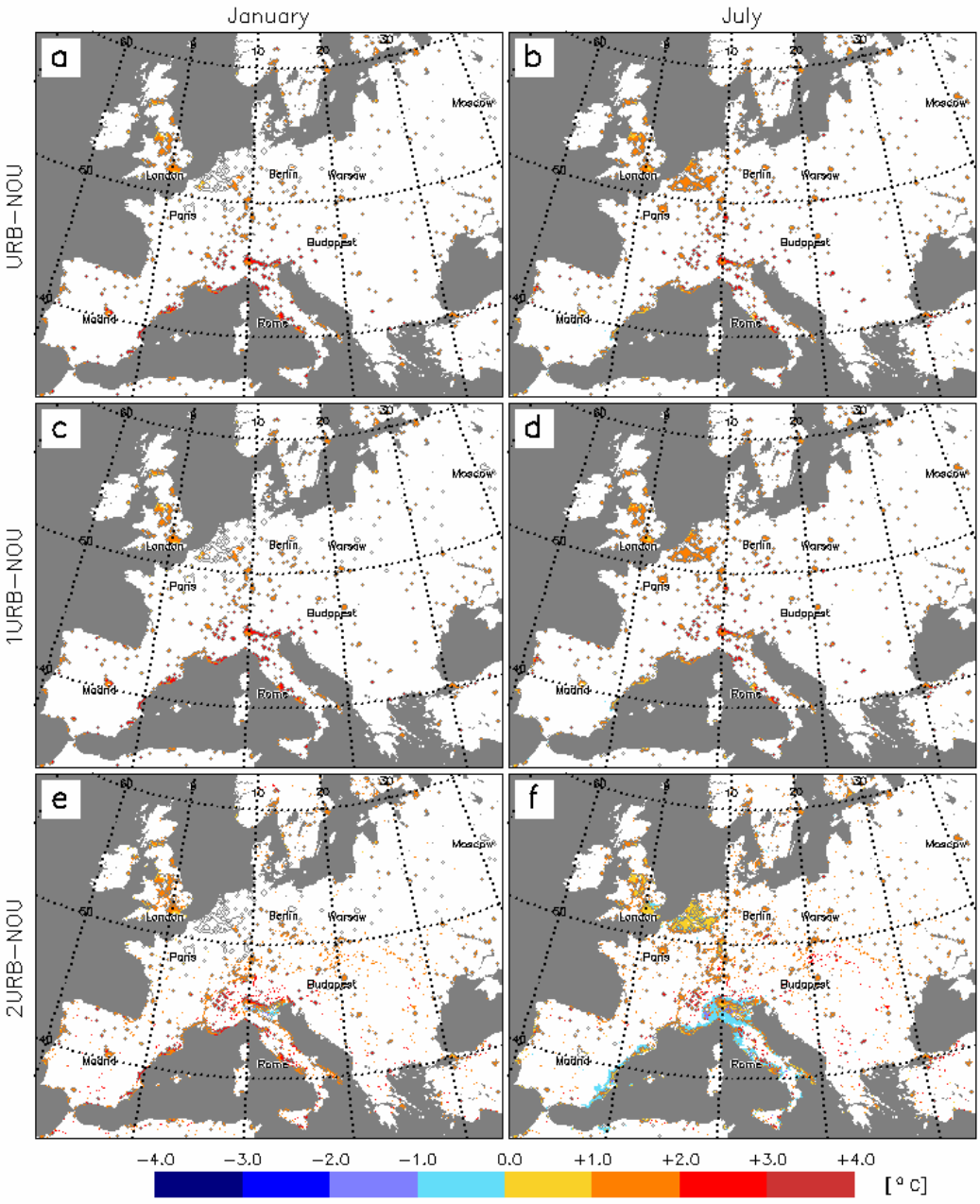

Figure 12. Differences in diurnal temperature range $Tmin_{URB\text{-}NOU}$ ((a) and (b)), $Tmin_{1URB\text{-}NOU}$ ((c) and (d)), $Tmin_{2URB\text{-}NOU}$ ((e) and (f)).

The increase of *Tmin* is attributed to the lack of air moisture and presence of additional anthropogenic heat sources, which result in frequent occurrence of UHI. While in URB and 1URB scenarios sources of urban heat are located in the same areas (urban masks match in this case), in the 2URB scenario the sources of anthropogenic heat and reduces moisture are more disperse. In this study it is assumed that the anthropogenic heat flux densities are not changing in any of urban growth scenarios. That means: with an increase of buildings height, the anthropogenic heat input per area is not changing, while the expansion of urban land leads to a larger input of anthropogenic heat into the atmosphere. This way of anthropogenic heat parameterisation is based on the assumption that living in closely connected urban clusters provides more efficient use of energy rather than living in low populated areas leads to energy waste (for commuting, individual heating etc.).

The Figure 12 shows that while URB and 1URB scenarios predict an increase of *Tmin* in most urban areas, 2URB scenario indicates some areas where *Tmin* declines. Especially this effect is evident in summertime simulation (Figure 12f). The most evident negative $Tmin_{2URB\text{-}NOU}$ is found in the vicinity of Milan urban area. In addition to this, the daily maximum temperature of this area reduces ($Tmax_{2URB\text{-}NOU}$) (Figure 13). A possible explanation for this cooling effect of the urban area of Milan, might be an increase of precipitation downwind from the city. However, significant increase of downwind precipitation occurs over a much smaller area (Figure 15) and cannot fully explain the reduction of *Tmin* and *Tmax* in rural surroundings near Milan. The reduction of rural temperatures was also found by Lamptey *et al*. (2005) in the eastern United States. However, this phenomenon needs further investigation.

Locally in places where the land use change takes place, $Tmax_{URB\text{-}NOU}$ and $Tmax_{1URB\text{-}NOU}$ are positive while surroundings largely exhibit temperature reduction ($Tmax_{URB\text{-}NOU}<0$; $Tmax_{1URB\text{-}NOU}<0$).

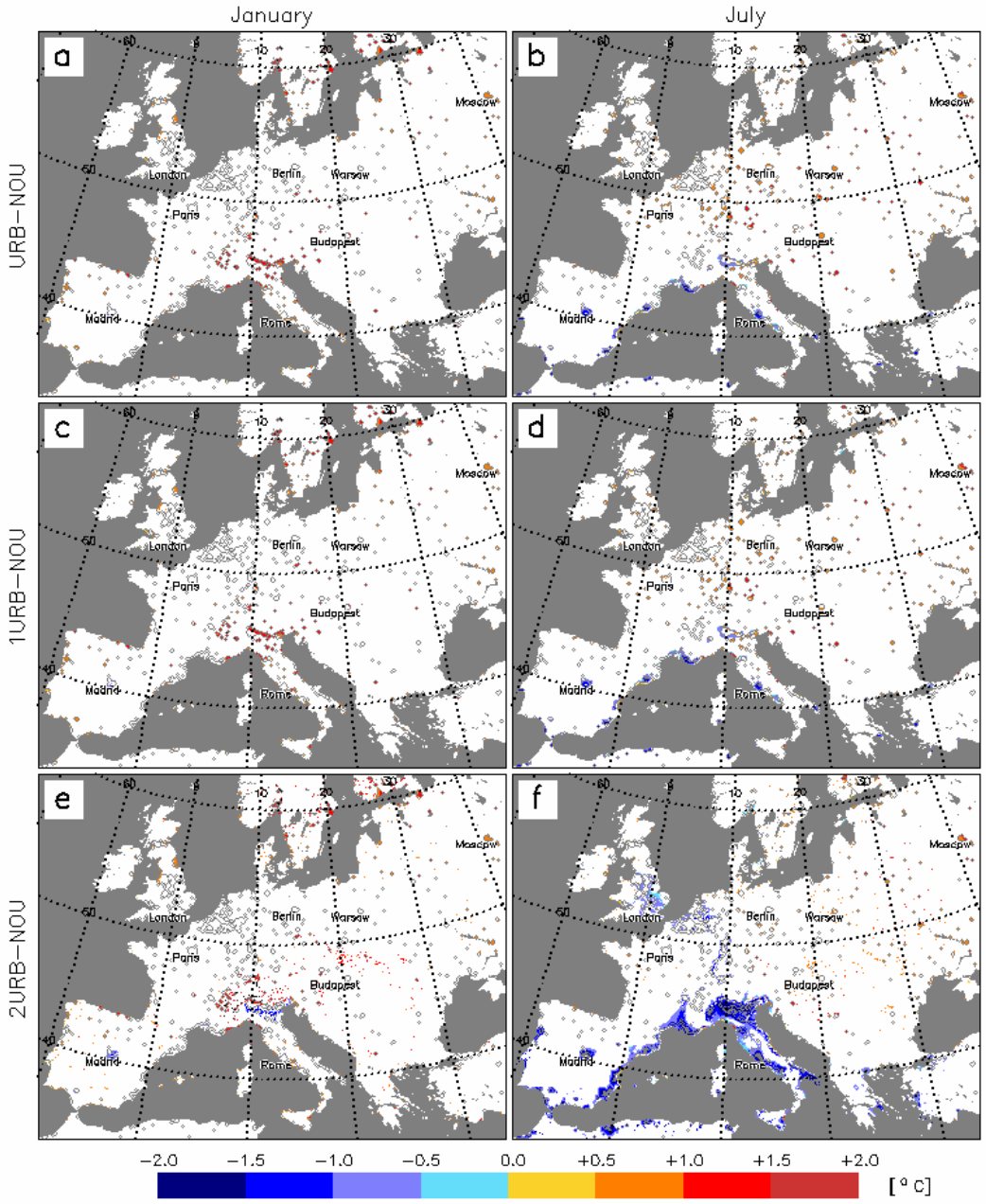

Figure 13. Differences in diurnal temperature range $Tmax_{URB-NOU}$ ((a) and (b)), $Tmax_{1URB-NOU}$ ((c) and (d)), $Tmax_{2URB-NOU}$ ((e) and (f)).

The differences between $Tmax_{1URB-NOU}$ and $Tmax_{URB-NOU}$ are small and are statistically insignificant (Figure 13, Table 10). The lower $Tmax_{1URB-NOU}$ than $Tmax_{URB-NOU}$ results from the larger shaded surfaces (walls, roads) in cities with smaller sky view factor where less solar radiation is absorbed by the urban canopy. The small differences in *Tmax* between URB and 1URB simulations mean that the effects on *Tmax* caused by actual urban areas and by urban areas with higher

buildings are of the same magnitude. However, the UCM scheme is forced by the wind speed field from the atmospheric model and calculates the surface resistance within the canyon. However, while the height of buildings is different in URB and 1URB simulations the distance between buildings does not change; this holds for the 2URB scenario as well. The distance between buildings governs the zero displacement height *z0* (Figure 14). In URB and 1URB scenarios *z0* is of the same order of magnitude and thus, there are no crucial differences in energy and momentum exchange between the urban canopy and the atmosphere in scenarios URB and 1URB, as well as in 2URB.

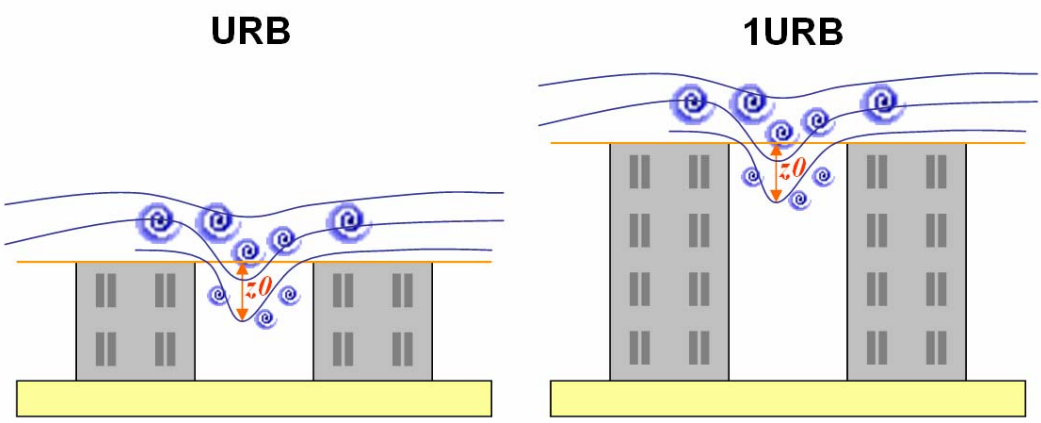

Figure 14. Urban canopy roughness length *z0* in URB and 1URB scenarios.

Differences of *Tmax* show large spatial variation (Figure 13). In July, a significant negative $Tmax_{URB\text{-}NOU}$ is found in Southern Europe while $Tmax_{URB\text{-}NOU}$ is positive in temperate climates (Figure 12). This effect persists in the 1URB and the 2URB scenarios as well (see "2.3.2. Effects of urban land cover on near-surface temperature" on page 25).

The mean $Tmax_{2URB\text{-}NOU}$ is larger than $Tmax_{URB\text{-}NOU}$ by +0.2-+0.6°C. This difference means that larger urban areas experience stronger urban cooling during day hours. However the uncertainty range of the *Tmax* differences is large and might explain this mismatch. To investigate this effect an analysis of longer time series might be needed.

These differences of minimum and maximum diurnal temperatures are attributed to changes in the geometrical and thermal properties of the perturbed areas and their energy balance (see "2.3.2. Effects of urban land cover on near-surface temperature" on page 25).

The largest differences in *Tmin*, *Tmax* and, *DTR* occur in urbanized areas of Southern Europe. A strong correlation of the $DTR_{urb\text{-}NOU}$ (*urb = URB|1URB|2URB*) to the monthly average temperature and precipitation is shown in the Table 11.

The $DTR_{urb\text{-}NOU}$ (*urb = URB|1URB|2URB*) strongly correlates to the temperature and precipitation in winter: the reduction of *DTR* is larger in dry, warm regions (the negative sign of the correlation coefficient means that the *DTR* reduction is larger for regions with higher monthly temperatures).

The correlation between the $DTR_{urb\text{-}NOU}$ (*urb = URB|1URB|2URB*) and the average monthly precipitation is strong in both seasons (Table 11). The positive correlation means that in the regions with higher monthly precipitation the $DTR_{urb\text{-}NOU}$ is smaller. The enlargement of urban areas leads to the expansion of the water-impenetrable land and increase of surface runoff into the cities' drainage system.

Table 11. Correlation coefficients between the diurnal temperature range (*DTR*) and climate variables. The stronger *DTR* reduction corresponds to the higher temperature and lower precipitation.

Variable	Correlation coefficient between *DTR* and average monthly temperature		Correlation coefficient between *DTR* and average monthly precipitation	
	January	July	January	July
$DTR_{URB\text{-}NOU}$	−0.43	−0.14	+0.30	+0.23
$DTR_{1URB\text{-}NOU}$	−0.42	−0.15	+0.30	+0.24
$DTR_{2URB\text{-}NOU}$	−0.42	−0.22	+0.23	+0.28

The correlation coefficients for each variable and season do not vary among scenarios by more than 0.07.

3.3.2. Effects of urban growth on precipitation

The daily precipitation differences between the base scenario and each of the urban scenarios, $PR_{URB\text{-}NOU}$, $PR_{1URB\text{-}NOU}$, $PR_{2URB\text{-}NOU}$, are highly variable over the whole domain (Figure 15). The areas where the differences in precipitation are found spread out far beyond cities' boundaries and the corresponding *REI* values exceed 5: significant differences in precipitation occur over a land area more than five times larger than the total urban area (Table 12).

Table 12. Regional Effect Index (*REI*) - ratio of the total area affected by the precipitation differences to the total urban area. The horizontal expansion of urban sprawl (2URB scenario) shows significantly larger *REI* values. Note: For URB and 1URB scenarios, urban area is the same while for 2URB scenario it is a twice-larger area.

Variable	*REI* in January	*REI* in July
$PR_{URB\text{-}NOU}$ *(mm day^{-1})*	6.38	5.79
$PR_{1URB\text{-}NOU}$ *(mm day^{-1})*	6.32	5.74
$PR_{2URB\text{-}NOU}$ *(mm day^{-1})*	7.29	6.16

The *REI* values for $PR_{URB\text{-}NOU}$ and $PR_{1URB\text{-}NOU}$ are of the same order of magnitude; this means, that the height of buildings is not a significant contributor to the precipitation change. Indeed, according to the model assumptions, the hydrological cycle (surface evaporation, surface runoff) and the buildings' height are not related directly. The largest *REI* values correspond to $PR_{2URB\text{-}NOU}$: the expanded impervious area alters larger neighbourhoods.

The average precipitation differences over land (model domain) are relatively small (Table 13). It is important to note that all urban scenarios (URB, 1URB, and 2URB) produced less precipitation than the base-line scenario (NOU). The large uncertainties of these numbers originate from the high spatial variability of the precipitation differences.

Table 13. Differences in precipitation (mm day^{-1}) between scenarios, which include urban land, and the base-line scenario. Note: For URB and 1URB scenarios, the urban area is the same while for 2URB scenario it is a twice as large area.

Variable	January		July	
	affected land	urban land	affected land	urban land
$PR_{URB\text{-}NOU}$	−0.02±0.16	+0.09±0.16	−0.22±0.65	−0.05±0.22
$PR_{1URB\text{-}NOU}$	−0.02±0.15	+0.09±0.16	−0.24±0.67	−0.04±0.21
$PR_{2URB\text{-}NOU}$	−0.07±0.19	+0.07±0.18	−0.54±0.89	−0.17±0.44

The daily precipitation depends on local climatic and orographic conditions. The $PR_{urb\text{-}NOU}$= 1 mm day^{-1} is of different degree of importance for a region with 5 mm day^{-1} on average and for a region with just 1.5 mm day^{-1}. To account for this, the relative precipitation difference is analysed. It is a dimensionless fraction (in percent) calculated as $\Delta PR_{urb\text{-}NOU} = PR_{urb\text{-}NOU} / PR_{NOU}$ ($urb = URB|1URB|2URB$) (Figure 15).

The $\Delta PR_{urb\text{-}NOU}$ ($urb = URB|1URB|2URB$) in urban areas have opposite trends in summer and winter: most urban sites exhibit a decreased rainfall in summer and an increased rainfall in winter (Table 13, Figure 15).

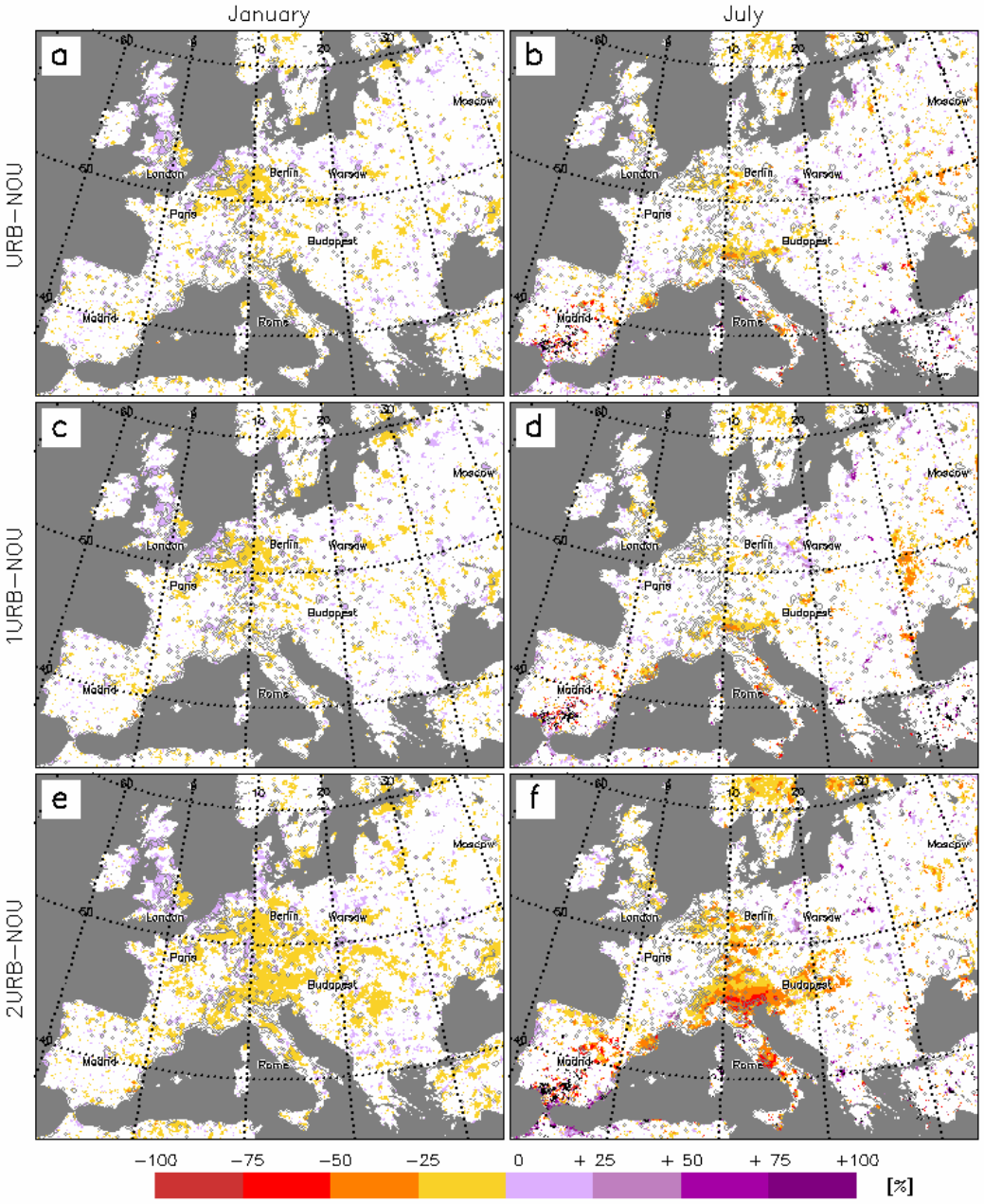

Figure 15. Differences in daily precipitation $\Delta PR_{URB\text{-}NOU}$ ((a) and (b)), $\Delta PR_{1URB\text{-}NOU}$ ((c) and (d)), $\Delta PR_{2URB\text{-}NOU}$ ((e) and (f)).

The enhanced winter precipitation over urban areas is caused by the additional heat sources (anthropogenic heat and UHI), which lead to enhanced convection (see

"2.3.3. Effects of urban land cover on precipitation", on page 30). In summertime, the reduced evaporation is the dominating factor in precipitation formation, which causes the precipitation reduction (see "2.3.3. Effects of urban land cover on precipitation", on page 30).

$\Delta PR_{URB\text{-}NOU}$ and $\Delta PR_{1URB\text{-}NOU}$ values have the same magnitude: 0 - +25% in Central European urban areas in winter, 0 - −25% in Southern European urban areas in summer. This similarity gives evidence that buildings' height is not a significant contributor to the magnitude of precipitation change. On the other hand, cities' size plays an important role: $\Delta PR_{2URB\text{-}NOU}$ indicates −25 - −50% reduction in daily precipitation in urbanized areas of Southern Europe e.g. Milan, Rome, Madrid, Barcelona and surroundings (Figure 15). This strong reduction is caused by the larger urban surface and, as follows, a larger water loss as runoff, which leads to the reduced available evaporation.

The correlation between $\Delta PR_{urb\text{-}NOU}$ ($urb = URB|1URB|2URB$) and the climate variables are analysed as for the diurnal temperature range. There is no correlation found between the $\Delta PR_{urb\text{-}NOU}$ ($urb = URB|1URB|2URB$) and climate variables in January and weak correlation (correlation coefficient << 0.1) in July.

Table 14. Correlation coefficients between daily precipitation differences and climate variables. While there is no correlation between $\Delta PR_{urb\text{-}NOU}$ ($urb = URB|1URB|2URB$) and the climate variables found in January and a weak correlation in July. '−' - no correlation is detected.

Variable	Correlation coefficient between *PR* and average monthly temperature		Correlation coefficient between *PR* and average monthly precipitation	
	January	July	January	July
$PR_{URB\text{-}NOU}$	−	0.003	−	-0.004
$PR_{1URB\text{-}NOU}$	−	0.016	−	-0.009
$PR_{2URB\text{-}NOU}$	−	0.025	−	-0.013

While the effects of the expanded urban land cover on precipitation are still relatively small, these effects might amplify with the further urban expansion and hence, should not be ignored in the future climate projections on local and regional scales.

3.4. Summary and outlook

This study suggested that the buildings' height does not significantly contribute to the regional climate, while the size of urban areas plays an important role in the spatial extent of temperature and precipitation disturbances.

The numerical simulations showed that larger cities affect larger rural areas by temperature and precipitation changes. The magnitude of the urban-induced temperature changes showed strong correlation with thermal regime: the reduction of the diurnal temperature range is largest in dry climates of Southern Europe. The reduction of diurnal temperature range is mainly driven by the increased night temperatures due to the urban heat island and limited surface evapotranspiration. This result is especially important for the development of urban heat island mitigation policies and predicting impacts of urban growth on the regional climate in different parts of Europe.

The effects on precipitation were found to be largely influenced by the expansion of urban sprawl. For both scenarios, the strongest reduction (more than 25%) of daily precipitation was found in July in Southern Europe in vicinity of large urban areas. The enlarged cities provided greater water surface runoff (into drainage systems) and caused stronger reduction of daily precipitation in summer. In January, urban areas experienced increased rainfall initiated by the enhanced convection, which resulted from the additional urban heat flux (anthropogenic and UHI).

Summarizing the results of this study:

- Larger cities affect larger rural territories by changes of near-surface temperatures and daily precipitation
- Larger urban areas cause greater reduction of precipitation in Southern Europe
- Height of a city's buildings does not significantly influence the magnitude and the spatial variability of the urban effects on the climate

This study assumed that growing urban areas do not change in structure (shapes and sizes of buildings, streets, urban vegetation etc.) and the effects estimated in this work originate only from the changes in cities' size. This encourages future research on predicting the dynamics of cities morphology and functioning (industry and traffic distribution, materials flow in/out of the city etc.) and possible climate responses to these dynamics. Such a study would require additional information of cities' pollution

and their inhabitants' behaviour, as well as highly precise urban land mapping (differentiation urban land use types, urban vegetation etc.).

4. Sensitivity of urban temperatures and precipitation to “green” urban planning strategies

4.1. Introduction

With progressing urbanization, the hot and dry urban climate conditions will affect a larger number of urban residents. As a result, the development of ecological approaches to mitigate the thermal stress is becoming very important.

Vegetated surfaces and open spaces help to improve the climate of towns, lowering the temperature by shading and evaporative cooling. The potential reduction of the city’s temperature by vegetation has been recorded in a number of studies (Bernatsky, 1982; Ca et al., 1998; Huang et al., 1987; Jauregui, 1991). However, various types of vegetation provide specific thermal and radiative properties of the canopy and may influence urban climate in different ways.

This chapter focuses on estimating contributions of two major types of a city’s vegetation, grassland and urban forest (mixed tree stand), to urban climate on local scale. The study is conducted for the urban areas of Berlin and Madrid using the modelling approach.

4.2. Materials and Methods

4.2.1. The model simulations

To isolate effects of vegetation contribution to the urban temperatures the regional model MM5 coupled to the urban canopy model UCM is used (see “1.2.2. Modifications of the land surface model” on page 3).

Two model scenarios represent urban areas with two different types of vegetation typically found in cities: 1) grass lawns, 2) mixed tree stands. Although urban vegetation is usually heterogeneous and includes a mixture of grass lawns, parks, and single trees, for simplicity only one type of vegetation is represented in each scenario. The fraction of vegetated urban land is set to 25% for both urban areas. Chosen vegetation types are expected to provide different thermal, radiative, and morphological properties of the canopy (Table 15) and are expected to contribute differently to the thermal regime of the lower atmosphere. To detect these

contributions, for each urban area two simulations are performed which correspond to the different urban vegetation type:

- GR25 simulation: urban vegetation is grass lawns which occupy 25 % of the total urban land
- TR25 simulation: urban vegetation is mixed tree stands which occupy 25 % of the total urban land

Table 15. Description of physical parameters for grassland and mixed forest vegetation types in urban areas.

Veg. cover Type	Simu-lation	Parameters of vegetation cover (summer and winter)									
		Albedo (%)		Moisture avail. (%)		Emissivity (%)		Roughness length (m)		Thermal inertia (cal cm^{-2} k^{-1} $s^{-1/2}$)	
Grassland	GR25	19.0	23.0	15.0	30.0	92.0	92.0	0.12	0.10	0.03	0.04
Mixed forest	TR25	13.0	14.0	30.0	60.0	94.0	94.0	0.50	0.50	0.04	0.06

Vegetation effects on urban thermal regimes can vary, depending on the climate of the area (see “2.3.2. Effects of urban land cover on near-surface temperature” on page 25 and “3.3.1. Effects of urban growth on near-surface temperature” on page 41). Urban areas of Berlin and Madrid are situated in temperate climate zone, but have different seasonal variations of temperature and precipitation (Table 16).

The Berlin urban area is situated in the area largely influenced by Humid Continental climate (Dfb climate class according to Köppen’s climate classification) a typical high-latitude city with strong seasonal temperature variations (from mild summers to cold winters) and excessive monthly precipitation throughout the year. The Madrid urban area is situated in the area Mediterranean climate (Cfb climate class according to Köppen’s climate classification) characterized by mild winters with excessive rains and hot dry summers.

Table 16. Climate characteristics of the Berlin and Madrid urban areas. The data are representative for the urban areas and suburban surroundings. "-" – no data available.

City name	Coordinates	Monthly mean temperature (°C)		Monthly total precipitation (mm)		Mean daily sunshine duration (h day^{-1})		Global radiation (kWh m^{-2} day^{-1})	
		Jan	Jul	Jan	Jul	Jan	Jul	Jan	Jul
Berlin	52.5°N 3.4°E	−0.4	+17.9	43.2	53.1	1.5	7.0	23	198
Madrid	40.5°N 3.5°W	+4.9	+24.2	38.0	12.0	4.9	12.3	-	-

For each of the two urban areas, the model runs are performed according to the suggested scenarios. Comparing results of the GR25 and TR25 simulations, differences in near-surface urban temperature and daily precipitation are analysed.

The model runs are restricted to periods of January and July of 2005 when strong effects of urban weather on atmospheric circulation can be expected significant effects of urban areas can be expected (see "2.2.4. Modelling Protocol" on page 20).

4.2.2. Analysis of model results

Comparing the diurnal temperatures variations retrieved from the two scenarios, the effects of the vegetation on the urban thermal regimes are analysed. Effects of vegetation on urban near-surface temperatures are detected as differences in the temperatures between corresponding scenarios. There is no statistical significance test applied to the data in this analysis due to the shortness of the data-series.

4.3. Results and Discussion

4.3.1. Effects of urban grassland versus forest on near-surface temperature

For the Berlin and Madrid urban areas, simulations show that the diurnal temperature range (*DTR*), calculated as the difference between the maximum (*Tmax*) and minimum (*Tmin*) diurnal temperature, is larger in the TR25 scenario than in the GR25 scenario (Table 17). These differences reach up to ~1°C for all simulations

except for the winter simulation for the Berlin urban area, where it accounts for only 0.1°C.

In the Berlin urban area in July, the minimum diurnal temperature in TR25 simulation is lower than in GR25 simulation by ~0.9°C; for the Madrid urban area, the TR25 minimum diurnal temperature is by ~0.1°C lower than in GR25 scenario (Table 17). That indicates an important contribution of the tree cover in Berlin to the night cooling and mitigation of the UHI by trees. One of the main causes of the UHI is the limited surface evaporation in cities, which inhibits the energy release from warm surfaces (see "2.3.2. Effects of urban land cover on near-surface temperature" on page 25). Tree stands have a larger water-holding capacity of the canopy and in the soil layers than grasses, providing higher the water availability for surface evaporation. Thus, trees help to reduce urban temperature by evaporative cooling by more than 1°C in the night hours in Berlin (Figure 16) in July.

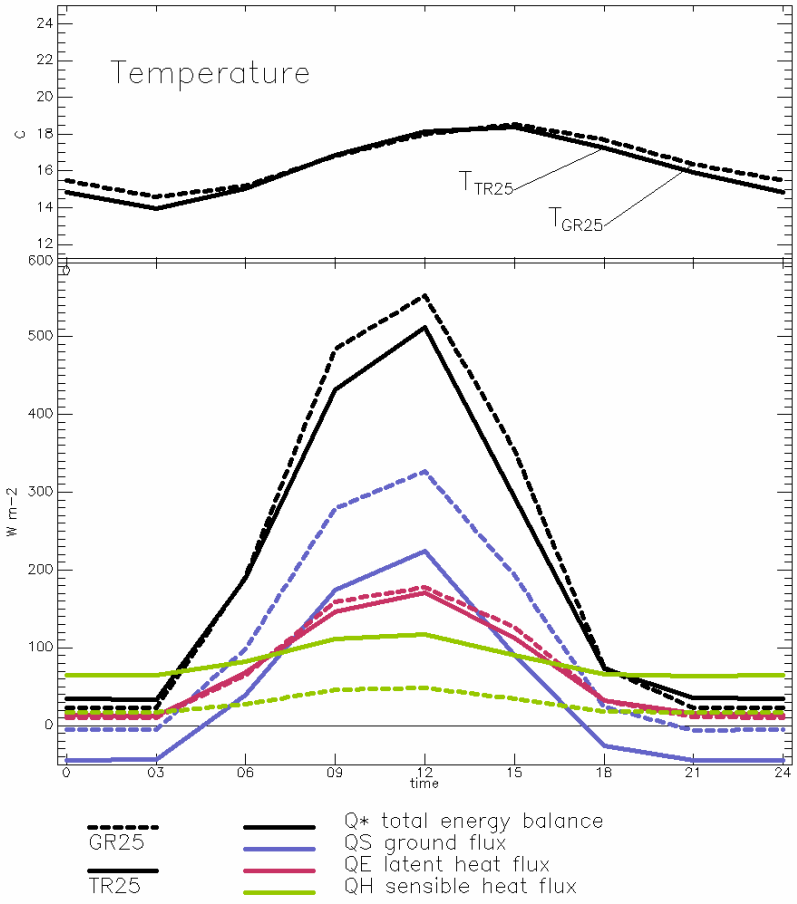

Figure 16. Synchronous energy balance of the Berlin urban site with forest (solid line) and grassland (dashed) as urban vegetation type. Data are 30-day averages over model simulation for July 2005.

However, the tree cover does not provide such strong night cooling in Madrid. This is explained by the scarce precipitation in the area of Madrid and high temperatures in summer (Table 16). The largest amount of precipitated water is evaporated to the warm dry atmosphere during daytime and is not stored in the canopy until the night time. This holds for the tree canopy as well as for the grass canopy. Because only little moisture is available for evaporative cooling in both canopies, no strong differences in UHI mitigation by trees and grass lawns can be found. In other words, if the urban environment experiences a drought, tree cover does not help to reduce night temperatures.

Table 17. Diurnal maximum (*Tmax*) and minimum temperature (*Tmin*), and the diurnal temperature range (*DTR*) for Berlin and Madrid urban areas. Each value is calculated as average and standard deviation of 30-day model simulation.

City	Month	Scenario	*Tmax* (°C)	*Tmin* (°C)	*DTR* (°C)
Berlin	Jan	GR25	+5.97±0.13	−6.35±0.23	12.32±0.11
		TR25	+5.93±0.43	−6.52±0.48	12.45±0.16
	Jul	GR25	+18.71±0.44	+4.34±0.49	14.37±0.26
		TR25	+18.82±0.69	+3.49±0.49	15.33±0.36
Madrid	Jan	GR25	+8.31±1.48	−5.63±1.19	13.94±0.61
		TR25	+8.52±1.61	−6.36±1.27	14.87±0.65
	Jul	GR25	+26.83±2.32	+9.51±1.99	17.32±0.58
		TR25	+27.63±2.35	+9.37±2.00	18.26±0.59

In January, *Tmin* in Madrid in the TR25 scenario is by ~0.7°C lower than in GR25 simulation while in Berlin the difference accounts for ~0.2°C only (Table 17). The reason for the smaller differences in the minimum diurnal temperature between TR25 and GR25 scenarios in Berlin is the presence of snow cover. The leafless trees and grasslands under snow interact with the lower atmosphere not directly but through the snow layer: both canopies are highly reflective and have a great proportion of water stored in the form of snow.

For both urban areas, the TR25 simulation shows higher *Tmax* by ~0.1°C than the GR25 simulation except for the July temperatures in Madrid (Table 17). The large uncertainties for differences of the *Tmax* between TR25 and GR25 scenarios result from high spatial variability of *Tmax* values (Figure 17). The total positive effect of

Tmax due to tree cover results from the urban pixels, which experience strongly higher *Tmax* in TR25, and this effect cancels out the negative effect in other urban pixels when averaged over the whole urban area.

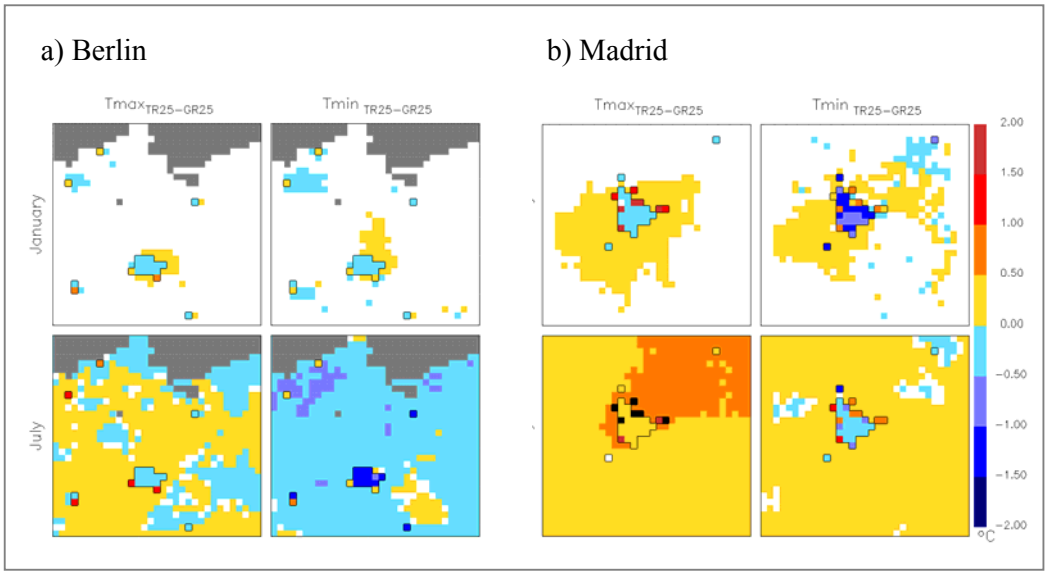

Figure 17. Difference of minimum and maximum diurnal temperatures between scenarios TR25 and GR25 for Berlin (a) and Madrid (b) urban areas. The urban forest (TR25) provides lower minimum diurnal temperatures (shown in blue colour) in both urban areas and higher maximum diurnal temperature in Madrid (shown in red colour).

This lower *Tmax* provided by urban forest originates from the differences in thermal and morphological properties of the canopy. In contrary to the grass lawns, the tree cover has higher volumetric heat capacity (thermal inertia) and is able to store more heat in the canopy (tree stems, tree crowns, air) than the grass canopy (Table 15) and thus, the tree canopy "needs" a larger heat input to reach a certain temperature than the grass canopy. The tree canopy generally has a larger volume per area unit and serves as a more efficient thermal isolator between the atmosphere and the land surface.

4.3.2. Effects of vegetation cover on precipitation

No large influence of the vegetation type on the precipitation is found. The precipitation differences for Berlin and Madrid within urban areas in both simulated seasons are less than 0.05 mm day^{-1} (Table 18). This small effect could be expected because the urban vegetation fraction is the same in GR25 and TR25 simulations and it is the only area of the potential water storage for the later evaporation. However, the

overall weak effect of the urban vegetation type to the urban precipitation can be also attributed to the small size of the vegetated area.

The precipitation differences over rural land are rather small although there is a strong positive precipitation anomaly in the north of Germany (**Error! Reference source not found.**) on the coast of Baltic Sea. It is attributed to the high vulnerability of the numerical model, which provides high uncertainty in its output in coastal zones and might be explained by the regional model's "butterfly" effect (numerical divergence), i.e. a high uncertainty in the predicted variable results from a relatively small uncertainty in the initial state of the model like land cover modification.

Table 18. Daily precipitation *PR* (mm day^{-1}) for Berlin and Madrid urban areas. Data are 30-day averages from the model simulation.

City	month	Scenario	*PR* (mm day^{-1})
Berlin	Jan	GR25	3.57±0.68
		TR25	3.53±0.65
	Jul	GR25	2.91±0.51
		TR25	2.87±0.92
Madrid	Jan	GR25	0.48±0.37
		TR25	0.48±0.38
	Jul	GR25	0.03±0.05
		TR25	0.06±0.10

The highly variable precipitation patterns can not be analysed on statistical significance

4.4. Summary and outlook

This study suggested that tree stands in cities provide a stronger cooling of urban environments than urban grass lawns of the same size.

The numerical simulations showed that the replacing of urban lawns by trees would result in a lowering of near-surface temperatures and help to mitigate the urban heat island. The temperature reduction is especially evident in the night hours and may be important for the city-planning in the future development with respect to the choice of urban vegetation.

The urban areas of Berlin and Madrid showed different degree of importance of the urban vegetation type for the city's thermal regime. In Madrid, the greater contribution of tree cover to the night cooling was found in wintertime, while in dry hot summer the role of vegetation type for night temperatures was minor. In Berlin, reversely to Madrid, the role of tree cover in night cooling was greatest in summertime, while it was hardly seen in wintertime when snow cover was present. Both cities showed minor effects of the vegetation type on precipitation.

Although, the results found in this study were not tested on statistical significance due to the short time series of the model data, it was found that a city's vegetation might be an important driving factor for the urban thermal regime through mitigation of the urban heat island. However, while looking at urban temperatures and the water cycle only, this study omitted the carbon cycle altered by urban environments, which plays an important role for urban vegetation dynamics and urban air quality. The role of vegetation as a potential sink or source of urban CO_2 is not well studied yet and encourages for the future investigations on the urban carbon cycle and contributions of urban pollution to the carbon balance of rural surroundings.

5. The response of the terrestrial biosphere to urbanization-driven changes in land use, climate and CO_2 and NO_x pollution.

5.1. Introduction

Urbanization alters the landscape by the replacing of vegetated land by urban land covered with buildings, roads, and extensive areas of impervious surfaces (parking lots, airports etc.), which reduce the potential carbon sink. As urban areas continue to grow the potential carbon sink is shrinking. Although urban areas occupy a small land fraction of about 2-3 % of Earth's surface, they are point-sources of about 90 % of anthropogenic carbon dioxide (CO_2) globally and of about 70 % attributed to traffic nitrogen dioxide emissions in Europe (USGS, 1999). However, while emissions of large industrial sources can be estimated from available inventories or monitored directly, diffuse area sources (traffic, residential heating/cooling) are poorly quantified.

Attempts to quantify the role of urban areas on the global carbon budget have focused largely on emissions inventories and sequestration in urban ecosystems. Many studies focused on different aspects of urbanization and on its effects on our environment such as land use modifications (USGS, 1999), global climate change (Jones et al., 1990; Kukla et al., 1986; Parker, 2004; Wood, 1988), regional and local climate modifications (Lamptey et al., 2005; Trusilova et al., peer review-b), atmosphere pollution (ESA, 2004; Idso et al., 2001; Koerner and Klopatek, 2002; WRI, 1998), water pollution (WRI, 1998), and impacts on human health (Granum and Løvik, 2002; Grigg, 2002; Van der Zee et al., 1999; WRI, 1998).

It was found that the enrichment of atmospheric CO_2 results in an increase on Net Primary Productivity (NPP) of plants (Idso, 1999; Idso and Kimball, 2001; Saxe et al., 1998) as well as the nitrogen fertilizers do, while little research is done on investigating the combined effects of these two and the urban climate.

This study is an attempt to estimate the contribution of urban climate anomalies and presence of urban land in combination with the CO_2 and NO_x pollution on the net carbon flux in Europe using a biogeochemical terrestrial ecosystem model.

5.2. Materials and Methods

5.2.1. Model of the terrestrial ecosystem

The spatial version of the terrestrial ecosystem model BIOME-BGC (Running and Hunt, 1993; Thornton, 1998; Thornton et al., 2002; Trusilova et al., peer review-a) is used to estimate carbon fluxes from vegetation to the atmosphere. This process-based model is used on regional scales and is driven by prescribed meteorological data, elevation and soil data, land cover data of eight plant functional types, CO_2 atmospheric concentrations and the nitrogen dry atmospheric deposition. The model resolves carbon fluxes for vegetated areas only and does not include any explicit parameterization for urban land. Effects of urban areas are included in the model indirectly, by introducing some urbanization-driven bias into the input data used to drive the model: 1) meteorological fields (temperature and precipitation), 2) CO_2 concentration, and 3) nitrogen atmospheric deposition, 4) parts of infertile/barren urban land. The carbon fluxes in urban areas are calculated only for the vegetated fraction of urban area.

5.2.2. The model simulations

The spinup simulation of the BIOME-BGC model is done for the reference year 1800 with the CO_2 concentration set to the constant of 283 ppm, the nitrogen atmospheric dry deposition set to the constant of 0.0002 kg m^{-2} and the meteorological data of years 1958-1978 used repetitively throughout the simulation. The spinup run is done for each grid cell of the model domain until the carbon balance reached its equilibrium state.

After the spinup simulation, the model is driven from the equilibrium state in 1800 to 1958 with the meteorological data from 1958-1978 (used repetitively), preindustrial nitrogen deposition prescribed as a constant for each model grid cell (preindustrial nitrogen deposition map), and with the increasing yearly CO_2 atmospheric concentration (Figure 18).

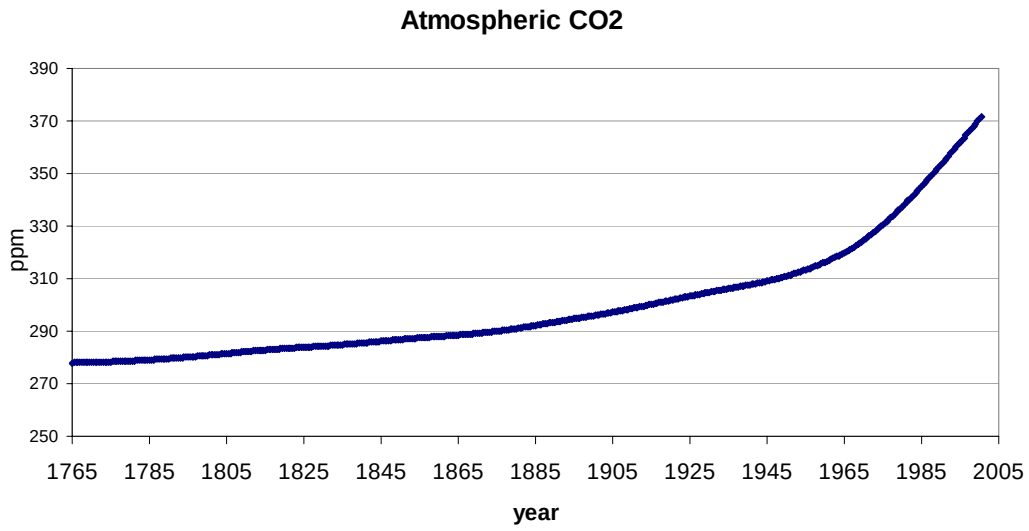

Figure 18. Background atmospheric CO_2 concentration input into the BIOME-BGC model. For each year one concentration value is provided, which represents an average CO2 concentration in the well-mixed atmosphere and is used for all model grid cells.

To isolate effects of individual urbanization factors on the carbon fluxes from the terrestrial biosphere during the time from 1958 to 2003, model simulations are performed according to six scenarios (Table 19), which represent different urbanization effects and their combination.

Table 19. Model scenarios representing different urban forcing on the terrestrial biosphere.

Simulation	Description
NOU	Base-line scenario; no urban CO_2 increase is used; Preindustrial nitrogen deposition is used; No urban area is present
URBLAND	As the base-line scenario, only the fraction of 0.25 of urban area is assumed to be vegetated and to contribute to the carbon balance; Areas occupied by impervious urban materials are excluded from the carbon balance calculation
URBMET	Urban temperature and precipitation anomaly
URBN	Industrial elevated nitrogen deposition
URBCO2	Urban CO_2 dome (increment in CO_2) concentration
URBALL	All urbanization factors from URBMET, URBLAND, URBN, and URBCO2

The NOU scenario is the base-line scenario, which represents a hypothetical situation with no urban land. It is used as the baseline scenario. Each of URBMET, URBLAND, URBN, and URBCO2 scenarios includes a single urban feature as urban climate, urban land, urbanization-driven atmospheric nitrogen deposition, and elevated carbon dioxide concentrations correspondingly. The URBALL scenario includes all three factors.

The model domain for this study covers area of 15°W-45°E 30°N-60°N with the spatial resolution of 0.25 degree. The BIOME-BGC model is driven by the meteorological data from 1958-2003 on a daily time step: minimum and maximum daily temperature, daily precipitation, downward shortwave solar radiation, and air relative humidity. The data was obtained by the regional model REMO (Jacob and Podzun, 1997) for multi-decadal atmospheric modelling for Europe (Feser et al., in preparation).

The data on the dry atmospheric nitrogen deposition used to drive the model was derived by a TM3 model (Heimann, 1995) run for preindustrial (before 1958) and industrial (year 1997) times (Figure 19) with NO_x sources in urban areas (the data was provided by an experimental simulation and is not published).

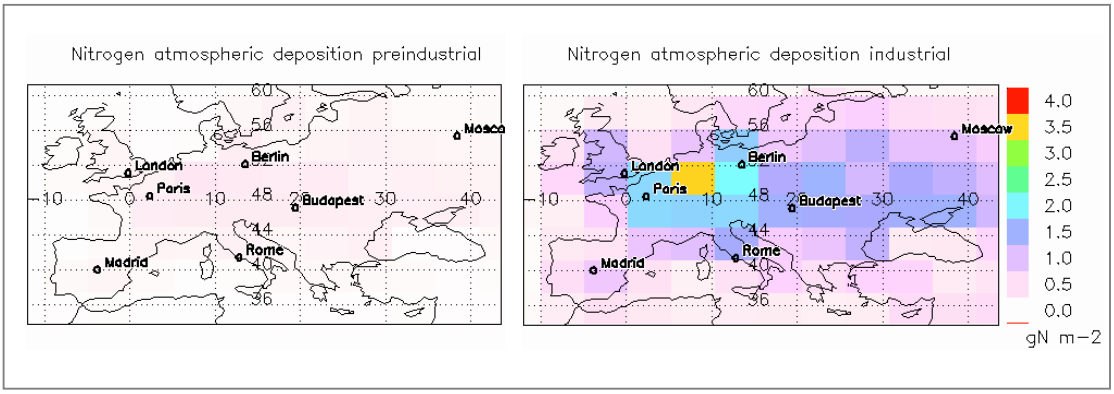

Figure 19. The maps of dry nitrogen atmospheric deposition were calculated with TM3 atmospheric transport model for the preindustrial (left) and industrial time (right).

The urban anomalies for temperature and precipitation are taken from the previous study (see "2.3.2. Effects of urban land cover on near-surface temperature" on page 25; "2.3.3. Effects of urban land cover on precipitation" on page 30) and added to the meteorological dataset which is used as input for the model.

The URBLAND scenario includes urban land as non-vegetated surfaces which do not participate in the carbon sequestration (Figure 20).

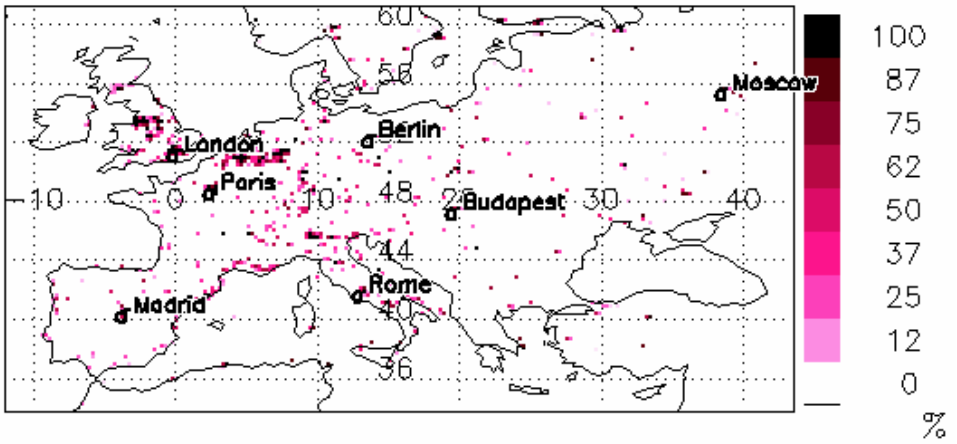

Figure 20. Urban land density as an input for the BIOME-BGC model. The fractional urban land density is derived from the upscaling and reprojecting of the urban mask given on the spatial resolution of 10 km (Lambert's conformal conic map projection) to the spatial resolution of 0.25 degree (Plate Carrée map projection). Value of 100 % means no vegetation in the grid cell; 0 % - no impervious land in the grid cell.

5.2.3. The urban CO_2 dome

The data of the CO_2 concentration for the period from 1958 to 2003 from the CARBOEUROPE-IP project is used to run the BIOME-BGC model. The data represents a smooth change in CO_2 concentration in the well mixed atmosphere and is used as the "background value". The carbon dioxide concentration within the model is updated with the annual time step using the same background value for all grid cells in one year. However, the urban areas change this homogeneous distribution by "hot spots" of intensive CO_2 release from diffuse area sources of anthropogenic origin (transport network, industrial emissions etc.).

It is known that urban areas expose higher CO_2 concentrations provided by exhaust from vehicles (Gratani and Varone, 2005; Idso et al., 2001; Idso et al., 2002; Nasrallah et al., 2003; Soegaard and Moller-Jensen, 2003; Velasco et al., 2005; Widory and Javoy, 2003; Zimnoch et al., 2004) , creating high CO_2 concentrations in the urban atmosphere called "urban CO_2-dome". The urban CO_2 is reported to be higher by 8 % to 129 % than rural CO_2 concentrations depending on season and location (Table 20).

Table 20. Observed CO_2 dome intensity in cities of Europe.

Site	CO_2 dome intensity	Source of information
Rome, Italy	15 % - 23 %	(Gratani and Varone, 2005)
Krakow, Poland	24 %	(Zimnoch et al., 2004)
Paris, France	Up to 220 %	(Widory and Javoy, 2003)
Copenhagen, Denmark	Up to 86 %	(Soegaard and Moller-Jensen, 2003)

Taking into account reported magnitude of the CO_2 dome it is assumed that the larger cities and more urbanized regions produce a CO_2 dome effect proportionally to the density of urban land. Using this assumption, the map of the carbon dioxide concentration increase (ΔCO_2) was calculated from the urban land density as a fraction (%) of the background CO_2 concentration value (Figure 21).

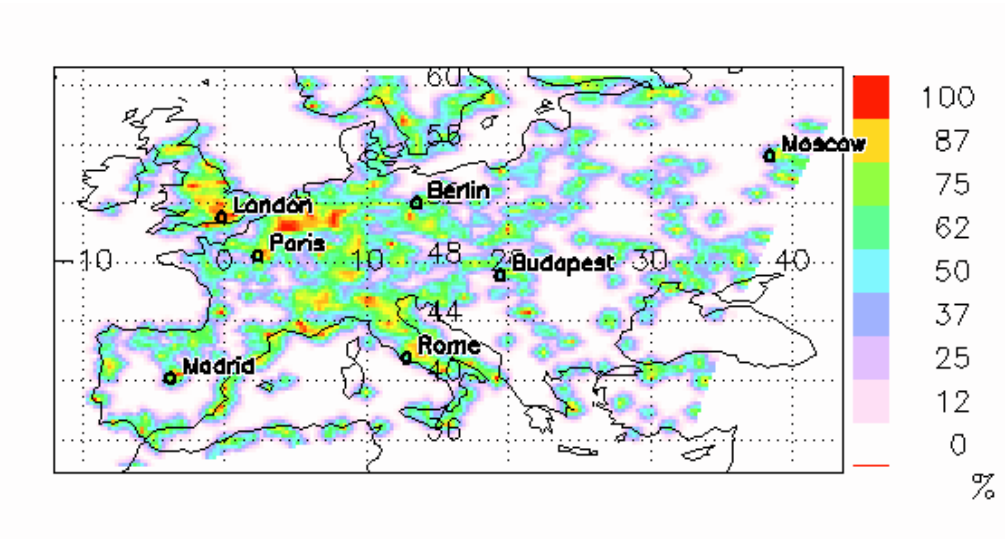

Figure 21. The spatial distribution of high carbon dioxide concentrations, which originate from urban areas (ΔCO_2) in % relatively to the background CO_2 concentration value.

The ΔCO_2 is used as an additional model input and is included into the calculation of input CO_2 concentration for each grid cell as:

$$Input\_CO_2 = Background\_CO_2 \cdot (1 + \Delta CO_2),$$

where

$Input\_CO_2$ is the CO2 concentration value for a grid cell

$Background\_CO_2$ is the input annual background carbon dioxide concentration (same value for all grid cells).

5.3. Results and Discussion

In order to quantify the response of carbon fluxes to the presence of urban land and urban pollution, results of the base-line (NOU) scenario and the URBALL scenario are compared. The URBALL scenario includes urban land, urban climate bias, urbanization-driven CO_2 and atmospheric nitrogen deposition and hence, represents the response of the terrestrial biosphere to the combination of these factors.

Various plant-functional types (PFTs) in different regions respond to the urban factors differently (Figure 22). The strongest increase of the carbon sink is found in areas with high nitrogen deposition and elevated urban CO_2 concentration: the industrial nitrogen deposition makes the pattern of flux differences strongly pronounced, while the footprint of the urban CO_2 increase is not clearly seen. According to the model setup, the fraction of 0.25 of urban areas is covered by vegetation. Only this fractional urban vegetated surface actively contributes to the carbon cycle. This explains the reduction of NEE (Figure 22) in areas with high urban land fraction (Figure 20). However, it is difficult to distinguish the effect on carbon sequestration from the urbanization-driven precipitation and temperature anomalies due to the discontinuity of these disturbances.

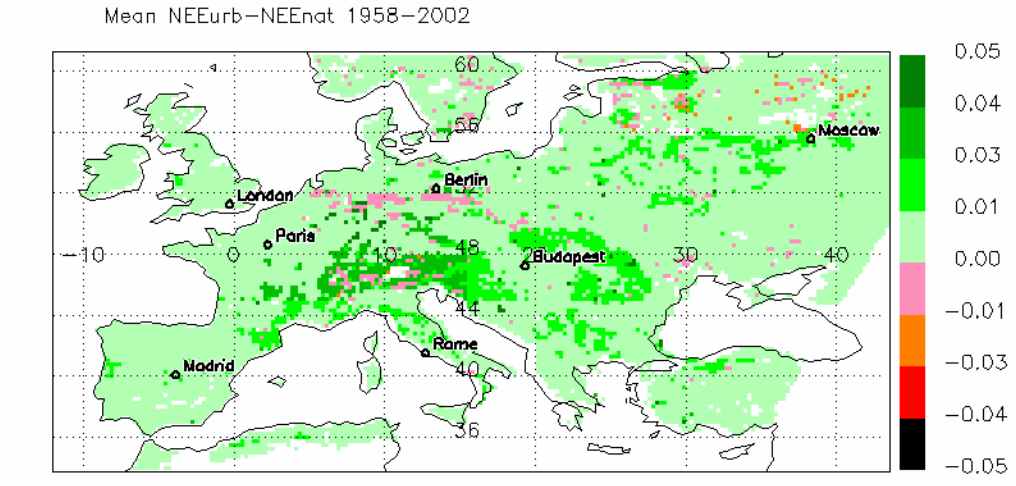

Figure 22. Response of the Net Ecosystem Exchange fluxes to the composition of all urbanization factors (URBALL scenario): anthropogenic nitrogen deposition, urban CO_2 concentration, presence of urban land, and the urban meteorological bias.

Comparison of URBALL and NOU model outputs do not provide enough information on how much each of the urbanization-driven environmental changes contributes individually to the change in carbon sequestration. In order to analyse the sensitivity of carbon fluxes to the individual urbanization factors the URBMET, URBLAND, URBN, and URBCO2 scenarios are be analysed.

The urban sparse vegetation cover (URBLAND) provides a reduction of GPP and RESP fluxes (−0.06 Pg year^{-1} each), but does not change the carbon balance (NEE)., because the vegetated land is simply replaced by no-sink no-source urban land. The urban meteorological anomalies (URBMET), i.e. reduced precipitation and near-surface warming, reduce the GPP of all vegetation types as well as the RESP fluxes by −0.22 Pg year^{-1} and by −0.23 Pg year^{-1} respectively. This is partly explained by the fact that the BIOME-BGC model is highly sensitive to the precipitation deficit. The elevated urban CO_2 concentrations (URBCO2) provide an increase of GPP and RESP and results in an increased carbon sink by +0.01 Pg year^{-1}. The increased atmospheric nitrogen deposition (URBN) acts as an efficient fertilizer and makes the largest contribution to the increased carbon sink (+0.07 Pg year^{-1}) of the vegetation as compared to other urbanization factors.

The combination of all urbanization factors acting at once (URBALL) results in an increase of GPP by +0.04 Pg year^{-1} due to the combined fertilization effects from the elevated urban CO_2 concentrations and the nitrogen deposition. The effect of the urban local meteorological bias are cancelled out by the urban fertilization effects on the vegetation and are not clearly distinguishable. The effect on the RESP is negative (−0.04 Pg year^{-1}) due to the removal of the vegetated land which is able to “respire” carbon. The increased GPP and reduced RESP result in an increased NEE by roughly +0.007 Pg year^{-1} to the combination of the considered urbanization-driven factors (Figure 23).

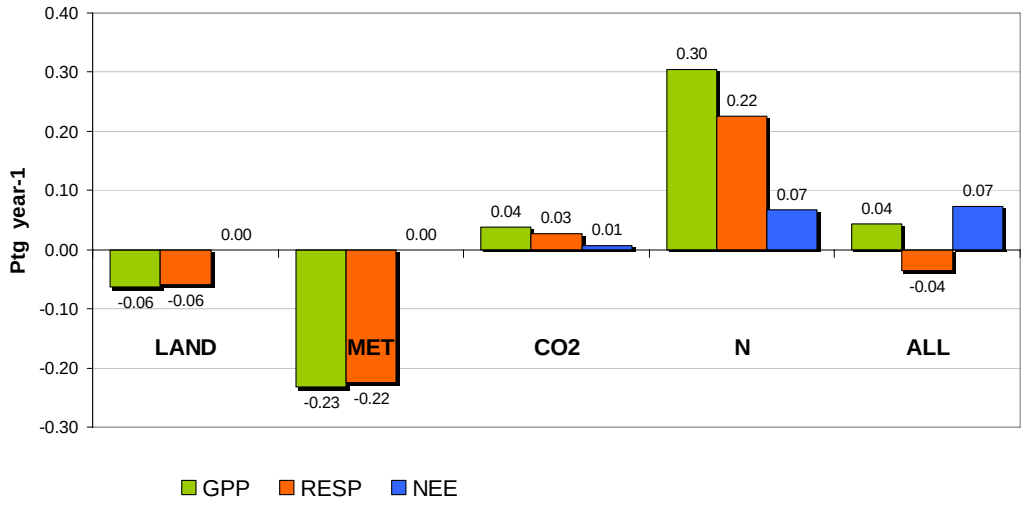

Figure 23. Response of carbon fluxes of vegetation in Europe to different urbanization factors: presence of urban land (LAND), urban meteorological bias (MET), urban CO_2-dome (CO2), anthropogenic nitrogen deposition (N) and composition of all four factors (ALL). Data are 46-year averages of BIOME-BGC model output (1958-2003).

From the Figure 23 it can be seen that the nitrogen atmospheric deposition alone provides the largest fertilization effect on the vegetation and by this it is likely to dominate the effect of the combination of all urbanization factors (URBALL). However, relationships between the carbon sequestration rates, nitrogen input, and climate variables are nonlinear. Because of this nonlinearity the total effect on vegetation of all urbanization factors together is not equal to the sum of individual effects of individual factors.

5.4. Summary and outlook

It was found that the removal of vegetation through urbanization reduced the potential carbon sink as well as the area of the ecosystem respiration and thus did not change the carbon balance.

The urbanization-driven climate change provided local reductions of the carbon sink due to the reduced urban precipitation in summer.

In contrary to the urban land and climate, the elevated CO_2 concentrations and the high nitrogen atmospheric deposition have shown fertilisation effects on the vegetation in Europe. Among the four considered factors of urbanization the elevated atmospheric nitrogen deposition, which originates from the transportation exhaust,

provided the largest contribution to the net carbon sink in Europe through the increase in carbon sequestration.

When all four urbanization disturbances were applied at the same time, the fertilization effects of the CO_2 and nitrogen pollution cancelled out the negative effects of urban land and climate on the total carbon balance. The combination of the four urbanization factors together resulted in an increase of the total carbon sink in Europe.

Summary

The first part of this study ("1. Representation of urban land in a regional model: modification of the Land Surface Scheme in the PSU/NCAR Mesoscale Weather Predicting Model (MM5)") demonstrated an important representation of urban areas in the mesoscale model.

In the second part ("2. Effects of urban land modifications on precipitation and near-surface temperature in Europe") it was shown that urban land contributes significantly to the local and regional climate. It was found that in summer urban areas experience reduced air moisture and high night temperatures as well as precipitation reduction. The strongest effects on near-surface temperature were found in warm dry climates of southern Europe during summertime. During winter time, urban surface warming leads to a more excessive urban precipitation, which results from the enhanced convection. This increase in the rainfall in urban areas is compensated by a reduced rainfall in rural areas.

The scenario which assumes urban growth showed that the expansion of urban land leads to a stronger reduction of diurnal temperature range. The expanded urban land provides a larger regional extent of urbanization-driven impacts on temperature and precipitation in both seasons (winter and summer). It was shown that an increase of buildings' height does not change near-surface temperatures and daily precipitation significantly.

It was found, that urban tree cover can significantly mitigate the night-time urban thermal stress as compared to urban grassland.

Among four urbanization-driven environmental disturbances the fertilization effects from the CO_2-dome and the atmospheric dry nitrogen deposition compensated for the negative contributions (carbon sink reduction) of the urban land use and the urban climate bias. The summary effect from the all four disturbances together resulted in an increase of the carbon sink in Europe.

Appendix 1

Physical parameters for vegetation categories and urban land use class of 25-category USGS classification for N.H. summer (Chen and Dudhia, 2001a; Chen and Dudhia, 2001b).

Integer ID	Description	Albedo	Moisture Avail.	Emissivity (at 9 μm)	Roughness Length (cm)	Thermal Inertia[17] (cal $cm^{-2}K^{-1}$ $s^{-1/2}$)
1	Urban	0.18	0.10	0.88	50.0	0.03
7	Grassland	0.19	0.15	0.92	12.0	0.03
9	Mixed Forest	0.13	0.30	0.94	50.0	0.04
23	Bare Grnd.	0.25	0.02	0.85	0.1	0.02

The heat transfer equation (5 layers) for internal temperatures of urban "surface":

$$C_1 \frac{\partial T_1}{\partial t} = \frac{1}{d_1}\left(\lambda_t(\Theta)\frac{\partial T}{\partial d_1}\right),$$

$$C_k \frac{\partial T_k}{\partial t} = \frac{1}{d_{k+1}}\left(\lambda_t \frac{\partial T}{\partial d_{k+1}}\right) - \frac{1}{d_k}\left(\lambda_t \frac{\partial T}{\partial d_k}\right), k = 1,..n \text{ , where}$$

n – number of soil layers;
d_k – thickness of the layer k (m);
Θ – fraction of unit soil volume occupied by water (dimensionless);
C_k – specific heat capacity of the kth layer as function of Θ (J m^{-3} K^{-1})
λ_t – thermal conductivity as function of Θ (W m^{-1} K^{-1});

[17] The term often used by engineers for modelling heat transfers when referring to the volumetric heat capacity

Appendix 2

Parameters of the TEB scheme (Masson, 2000).

Radiative parameters

Symbol	Designation	Value	Unit
Albedo			
α_R	Roof	0.15	-
α_r	Road	0.08	-
α_w	Wall	0.25	-
Emissivity			
ζ_R	Roof	0.90	-
ζ_r	Road	0.94	-
ζ_w	Wall	0.85	-

Thermal parameters

Symbol (k=1..3)	Designation	Value for layer *k*, *k*=1..3			Unit
		1	2	3	
Thickness of the *k*th layer					
d_{Rk}	Roof	0.050	0.400	0.050	m
d_{rk}	Road	0.050	0.100	1.000	m
d_{wk}	Wall	0.020	0.125	0.020	m
Thermal conductivity of the *k*th layer					
λ_{Rk}	Roof	1.5100	0.0800	0.0500	W m^{-1} K^{-1}
λ_{rk}	Road	0.7454	0.2513	0.2513	W m^{-1} K^{-1}
λ_{wk}	Wall	0.9338	0.9338	0.0500	W m^{-1} K^{-1}
Heat capacity of the *k*th layer					
C_{Rk}	Roof	2.11	0.28	0.29	10^6 J m^{-3} K^{-1}
C_{rk}	Road	1.94	1.28	1.28	10^6 J m^{-3} K^{-1}
C_{wk}	Wall	1.55	1.55	0.29	10^6 J m^{-3} K^{-1}

The heat transfer equation (3 layers) for internal temperatures of roof, wall, and road surfaces :

$$C_{*1}\frac{\partial T_{*1}}{\partial t} = \left(1-\delta_{snow*}\right)\frac{1}{d_{*1}}\left(S_* + L_* - H_* - LE_* - G_{*1,2}\right) + \delta_{snow*}\frac{1}{d_{*1}}\left(G_{*snow,1} - G_{*1,2}\right),$$

$$C_{*k}\frac{\partial T_{*k}}{\partial t} = \frac{1}{d_{*k}}\left(G_{*k-1,k} - G_{*k,k+1}\right), k = 1,..n \text{ , where}$$

*- roof, road or wall;
d_{*k} – thickness of the layer *k* (m);
δ_{snow} – fraction of the surface covered by snow (dimensionless);
C_{*k} – specific heat capacity of the *k*th layer (J m^{-3} K^{-1});
S_*,L_*,H_*,LE_*–net solar and infrared radiation, sensible and latent heat flux (W m^{-2});
$G_{*1,2}$ – conduction heat flux between the surface and the underlying layer (W m^{-2});
$G_{*1,snow}$ – conduction heat flux between the snow layer and the surface (W m^{-2});
$G_{*k-1,k}$ – conduction heat fluxes between the *k-1* and *k* layers (W m^{-2});
$G_{*k,k+1}$ – conduction heat fluxes between the *k* and *k+1* layers (W m^{-2});

Appendix 3

Underground runoff and surface runoff differences between URB and NOU scenarios.

The NOU scenario includes no urban area. The URB scenario represents "actual" state of urbanization as in 2000-2005.

Effects of urban land cover on the surface runoff (left) and underground runoff (right). In urban areas without vegetation the *surface runoff = underground runoff*, no soil layer is assumed to be under paved asphalt or concrete surfaces. The 15% vegetation fraction in the model set-up provides very little contribution to the surface runoff in urban areas.

SFCRUNOFF$_{URB-NOU}$ UGDRUNOFF$_{URB-NOU}$

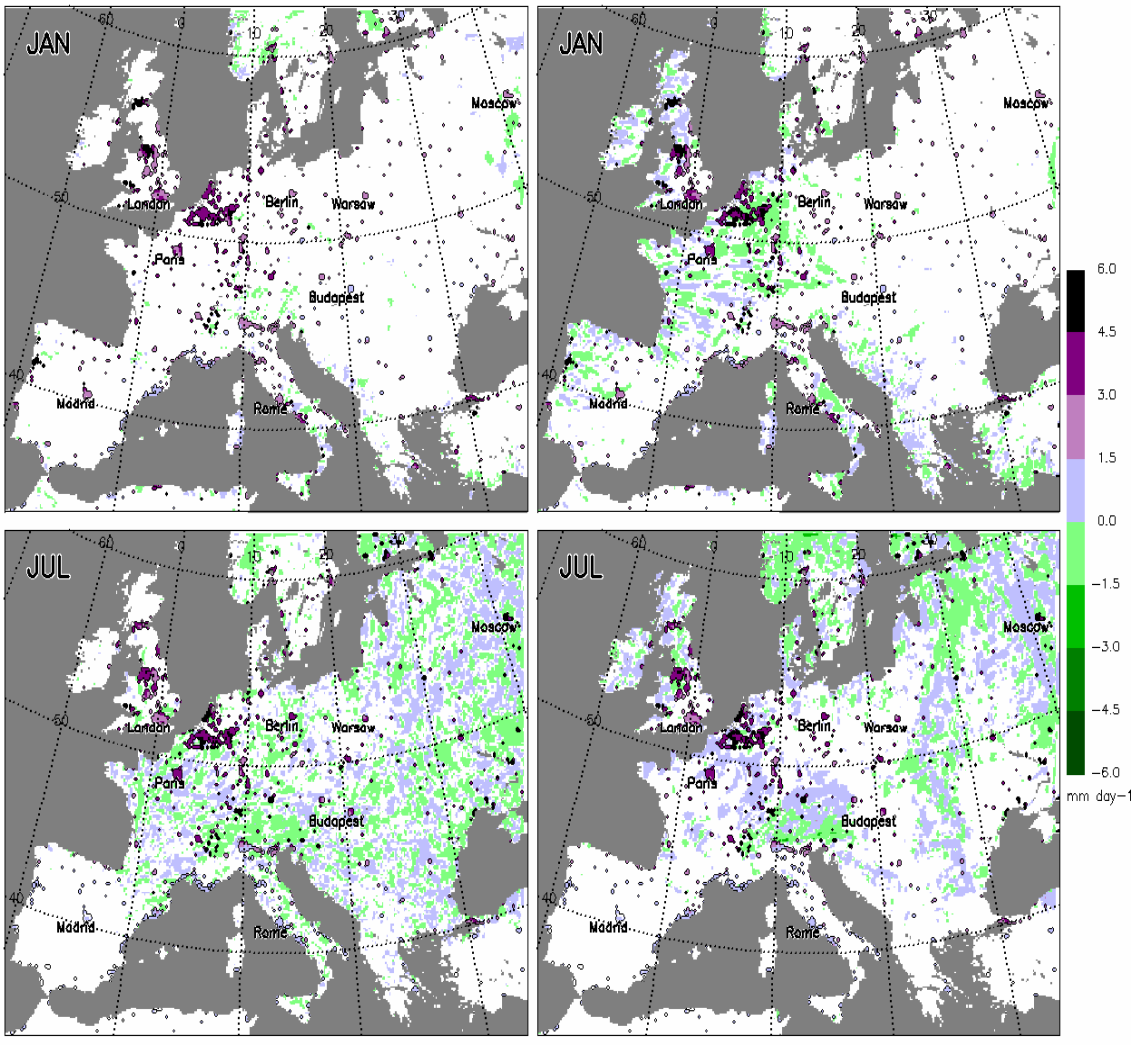

Appendix 4

Surface pressure differences between URB and NOU scenarios.

The NOU scenario includes no urban area. The URB scenario represents “actual” state of urbanization as in 2000-2005.

Due to increased urban near-surface temperatures and decreased air moisture, the lower atmosphere experiences an expansion and an increase in surface pressure (Pa). The strongest effect is found in highly urbanized areas.

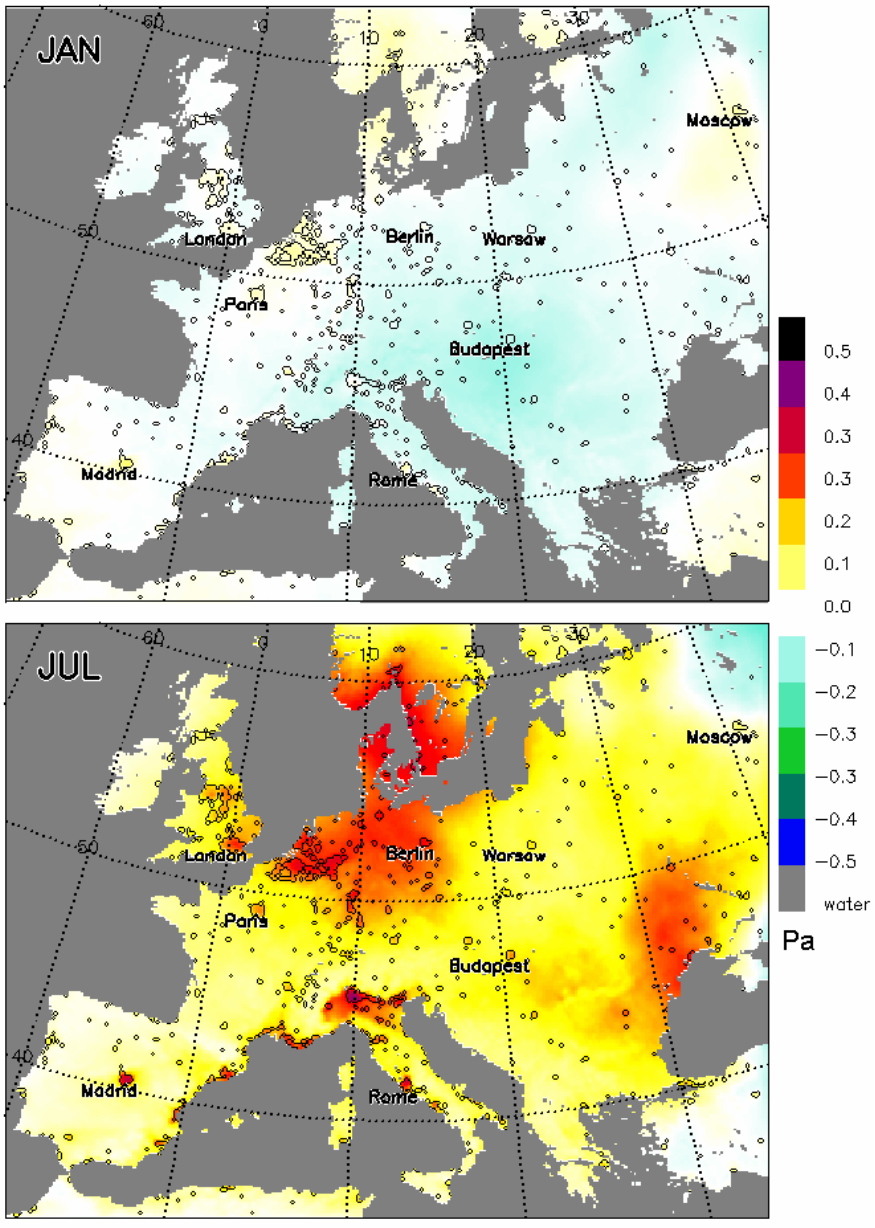

Appendix 5

Urban land masks.

All urban masks have spatial resolution of 10km and are used directly as input into the model.

- STD – urban mask in GLCC-USGS urban land cover map used in MM5 model
- URB – "actual" urban mask derived from urban score map; represents urban areas in Europe in the period 2000-2005
- 2URB – hypothetical urban mask; represents urban area as a result of horizontal expansion of urban sprawl

Urban mask	Number of urban pixels in the model domain	Total area (km^2)	Fraction of urban land in the total land in the model domain (%)
STD	186	$18.6 \cdot 10^3$	0.3
URB	1591	$159.1 \cdot 10^3$	2.8
2URB	2228	$222.8 \cdot 10^3$	3.9

The size of the model's grid cell is 100 km^2.
The total number of land pixels in the model domain is 57304 (~$5.7 \cdot 10^3$ km^2).

The ratio between the URB and the 2URB total urban areas holds 1:2 in countries of Western Europe where the CORINE land cover map was available for validation of the new urban mask URB. Once extended to the whole model domain which includes areas with lower densities or urban areas (Eastern Europe, Western Russia etc.), the ratio drops to 1.4:1.

References

Alonso, M.S., Labajo, J.L. and Fidalgo, M.R., 2003. Characteristics of the urban heat island in the city of Salamanca, Spain. Atmosfera: 137-148.

Atkinson, B.W., 2002. Numerical modelling of urban heat-island intensity. Department of Geography, Queen Mary, University of London, London E1 4NS, U.K.

Bernatsky, A., 1982. The contribution of trees and green spaces to a town climate. Energy and Buildings, 5: 1-10.

Best, M.J., 2005. Representing urban areas within operational numerical weather prediction models. Boundary-Layer Meteorology, 114: 91-109.

Borghi, S., Corbetta, G. and De Blase, L., 2000. A heat island model for large urban areas and its application to Milan. Il Nuovo Cimento, 23(5): 547-566.

Bottyan, Z., Kircsi, A., Szegedi, S. and Unger, J., 2005. The Relationship Between Built-up Areas and the Spatial Development of the Mean Maximum Urban Heat Island in Debrecen, Hungary. International Journal of Climatology, 25: 405-418.

Brunetti, M., Mangianti, F., Maugeri, M. and Nanni, T., 2000. Urban heat island bias in Italian air temperature series. Il Nuovo Cimento, 23(4): 423-431.

Ca, V.T., Asaeda, T. and Abu, E.M., 1998. Reduction of air conditioning energy caused by a nearby park. Energy and Buildings, 29: 83-92.

Changnon Jr., S.A., Shealy, R.T. and Scott, R.W., 1991. Precipitation changes in fall, winter, and spring caused by St. Louis. Journal of Applied Meteorology, 30: 126-134.

Chen, F. and Dudhia, J., 2001a. Coupling an Advanced Land Surface-Hydrology Model with the Penn State-NCAR MM5 Modeling System. Part I: Model Implementation and Sensitivity. American Meteorological Society, 129: 569-585.

Chen, F. and Dudhia, J., 2001b. Coupling an Advanced Land Surface-Hydrology Model with the Penn State-NCAR MM5 Modeling System. Part II: Preliminary Model Validation. Advances in Ecological Research, 129: 587-604.

Dixon, P.G. and Mote, T.L., 2003. Patterns and Causes of Atlanta's Urban Heat Island Initiated Precipitation. Journal of Applied Meteorology, 42(9): 1273-1284.

Dudhia, J., 1989. Numerical study of convection observed during the winter monsoon experiment using a mesoscale two-dimensional model. Journal of the Atmospheric Sciences, 46(20): 3077-3107.

Ek, M.B. et al., 2003. Implementation of Noah land surface model advances in the National Center for Environmental Prediction operational mesoscale Eta model. Journal of Geophysical Research, 108(D22): 8851.

Elvidge, C.D. et al., 1999. Radiance Calibration of DMSP-OLS Low-light Imaging Data of Human Settlements. Remote Sensing of Environment, 68(1): 77-88.

Elvidge, C.D. et al., 1997. Satellite Inventory of Human Settlements Using Nocturnal Radiation Emissions: A Contribution for the Global Toolchest. Global Change Biology, 3(5): 387-395.

ESA, 2004. NO2 pollution characteristic for Europe's sprawled urban areas: Nitrogen dioxide pollution. European Space Agency.

Feser, F., Weisse, R. and von Storch, H., in preparation. Multi-decadal Atmospheric Modeling for Europe Yields Multi-purpose Data.

Gonzalez, J.E. et al., 2005. Urban heat islands developing in coastal tropical cities. EOS, Transactions, American Geophysical Union, 86: 397,403.

Granum, B. and Løvik, M., 2002. The Effect of Particles on Allergic Immune Responses. Toxicological Sciences, 65(1): 7-17.

Gratani, L. and Varone, L., 2005. Daily and seasonal variation of CO2 in the city of Rome in relationship with the traffic volume. Atmospheric Environment, 39: 2619-2624.

Grell, G.A., Dudhia, J. and Stauffer, D.R., 1995. A Description of the Fifth-Generation Penn State/NCAR Mesoscale Model (MM5), NCAR Tech. Note, pp. 122.

Grigg, J., 2002. The health effects of fossil fuel derived particles. Archives of Disease in Childhood, 86: 79-83.
Grimmond, C.S.B. and Oke, T.R., 1999. Evapotranspiration rates in urban areas, Impacts of Urban Growth on Surface Water and Groundwater Quality. IAHS, Birmingham.
Heimann, M., 1995. The TM2 tracer model, model description and user manual. 10, Deutsches Klimarechenzentrum, Hamburg.
Hong, S.-Y. and Pan, H.-L., 1996. Nonlocal boundary layer vertical diffusion in a medium-range forecast model. Monthly weather review, 124: 2322-2339.
Huang, Y.J., Akbari, H., Taha, H. and Rosenfeld, A.H., 1987. The potential of vegetation in reducing summer cooling loads in residential buildings. Journal of Climate and Applied Meteorology, 26: 1103-1116.
Huff, F.A. and Changnon Jr., S.A., 1973. Precipitation Modification By Major Urban Areas. Bulletin of the American Meteorological Society, 54(12): 1220-1232.
Hupfer, P. and Chmielewski, F.M., 1990. Das Klima von Berlin.
Idso, C.D., Idso., S.B. and Balling Jr., R.C., 2001. An intensive two-week study of an urban CO2 dome in Phoenix, Arizona, USA. Atmospheric Environment, 35: 995-1000.
Idso, S.B., 1999. The long-term response of trees to atmospheric CO2 enrichment. Global Change Biology, 5: 493-495.
Idso, S.B., Idso, C.D. and Balling Jr., R.C., 2002. Seasonal and diurnal variations of near-surface atmospheric CO2 concentrations within a residential sector of the urban CO2 dome of Phoenix, AZ, USA. Atmospheric Environment, 36: 1655-1660.
Idso, S.B. and Kimball, B.A., 2001. CO2 enrichment of sour orange trees: 13 years and counting. Environmental and Experimental Botany, 46: 147-153.
Imhoff, M.L., Lawrence, W.T., Stutzer, D.C. and Elvidge, C.D., 1997. A Technique for Using Composite DMSP/OLS "City Lights" Satellite Data to Accurately Map Urban Areas. Remote Sensing of Environment, 61(3): 361-370.
Jacob, D. and Podzun, R., 1997. Sensitivity studies with the regional climate model REMO. Meteorology and Atmospheric Physics, 63: 119-129.
Jauregui, E., 1991. Influence of a large urban park on temperature and convective precipitation in a tropical city. Energy and Buildings, 15-16: 457-463.
Jin, M., Dickinson, R.E. and Zhang, D.L., 2005. The Footprint of Urban Areas on Global Climate as Characterized by MODIS. American Meteorological Society: 1551-1565.
Jones, P.D. et al., 1990. Assessment of urbanization effects in time series of surface air temperature over land. Nature, 347: 169-172.
Kalnay, E. and Cai, M., 2003. Impacts of urbanization and land-use change on climate. Nature, 423: 528-531.
Klysik, K. and Fortuniak, K., 1999. Temporal and spatial characteristics of the urban heat island of Lodz , Poland. Atmospheric Environment, 33: 3885-3895.
Koerner, B. and Klopatek, J., 2002. Anthropogenic and natural CO2 emissions sources in arid urban environment. Environmental Pollution, 116: S45-S51.
Kukla, G., Gavin, J. and Karl, T.R., 1986. Urban Warming. American Meteorological Society: 1265-1270.
Kusaka, H., Hiroaki, K., Yokihiro, K. and Fujio, K., 2001. A simple single-layer urban canopy model for atmospheric models: comparison with multi-layer and slab models. Boundary-Layer Meteorology, 101: 329-358.
Kusaka, H. and Kimura, F., 2004. Thermal Effects of Urban Canyon Structure on the Nocturnal Heat Island: Numerical Experiment Using a Mesoscale Model Coupled with an Urban Canopy Model. American Meteorological Society, December: 1899-1910.
Lamptey, B.L., Barron, E.J. and Pollard, D., 2005. Impacts of agriculture and urbanization on the climate of the Northeasten United States. Global and Planetary Change, 49: 203-221.
Lavalle, C. et al., 2002. Towards an urban atlas, European Environment Agency, Copenhagen.

Loveland, T.R. et al., 2000. Development of a global land cover characteristics database and IGBP DISCover from 1 km AVHRR data. International Journal of Remote Sensing, 21: 1303-1330.
Martilli, A., Clappier, A. and Rotach, M.W., 2002. An Urban Surface Exchange Parameterisation for Mesoscale Models. Boundary-Layer Meteorology, 104: 261-304.
Masson, V., 2000. A physically-based scheme for the urban energy budget in atmospheric models. Boundary-Layer Meteorology, 94: 357-397.
Masson, V., Grimmond, C.S.B. and Oke, T.R., 2002. Evaluation of the Town Energy Balance (TEB) Scheme with Direct Measurements from Dry Districts in Two Cities. Journal of Applied Meteorology, 41(10): 1011-1026.
Mayer, H., Matzarakis, A. and Iziomon, M.G., 2003. Spatio-temporal variability of moisture conditions within the Urban Canopy Layer. Theor. Appl. Climatol., 76: 165-179.
Montavez, J.P., Rodriguez, A. and Jimenez, J.I., 2000. A Study of the Urban Heat Island of Granada. International Journal of Climatology, 20: 899-911.
Müller, M., 1983. Handbuch ausgewählter Klimastationen der Erde.
Nasrallah, H.A., Balling Jr., R.C., Madi, S.M. and Al-Ansari, L., 2003. Temporal variations in atmospheric CO2 concentrations in Kuwait City, Kuwait with comparisons to Phoenix, Arizona, USA. Environmental Pollution, 121: 301-305.
Oke, T.R., 1982. The energetic basis of the urban heat island. Quarterly Journal Royal Meteorological Society, 108: 1-24.
Oke, T.R., 1988. The Urban Energy Balance. Progress in Physical Geography, 12(471-508).
Parker, D.E., 2004. Large-scale warming is not urban. Nature, 432: 290.
Rosenfeld, D., 2000. Suppression of rain and snow by urban and industrial Air Pollution. Science, 287(10): 1793-1796.
Running, S.W. and Hunt, E.R., 1993. Generalization of a forest ecosystem process model for other biomes Biome-BGC. Bulletin of the Ecological Society of America, 72(2 SUPPL): 236.
Saxe, H., Ellsworth, D.S. and Heath, J., 1998. Tree and forest functioning in an enriched CO2 atmosphere. New Physiologist, 139: 395-436.
Shepherd, M.J. and Jin, M., 2004. Linkages Between the Built Urban Environment and Earth's Climate System. EOS, 85(23): 227-228.
Shepherd, M.J., Pierce, H. and Negri, A.J., 2002. Rainfall Modification by Major Urban Areas: Observations from Spaceborne Rain Radar on the TRMM Satellite. Journal of Applied Meteorology, 41(7): 689-701.
Soegaard, H. and Moller-Jensen, L., 2003. Towards a spatial CO2 budget of a metropolitan region based on textural image classification and flux measurements. Remote Sensing of Environment, 87: 283-294.
Thornton, P.E., 1998. Regional Ecosystem Simulation: Combining Surface- and Satellite-Based Observations to Study Linkages between Terrestrial Energy and Mass Budgets, University of Montana, Missoula.
Thornton, P.E. et al., 2002. Modeling and measuring the effects of disturbance history and climate on carbon and water budgets in evergreen needleleaf forests. Agricultural and Forest Meteorology, 113(1-4): 185-222.
Trusilova, K. et al., peer review-a. Parameter estimation for the terrestrial ecosystem model BIOME-BGC using nonlinear inversion. Ecological Modelling.
Trusilova, K. et al., peer review-b. Urbanization Impacts on the Climate in Europe. Journal of Applied Meteorology and Climatology.
Unger, J., Suemeghy, Z. and Zoboki , J., 2001. Temperature cross-section features in an urban area. Atmospheric Research, 58: 117-127.
USGS, 1999. Analyzing Land Use Change In Urban Environments, U.S. Department of the Interior; U.S. Geological Survey.
Van der Zee, S. et al., 1999. Acute effects of urban air pollution on respiratory health of children with and without chronic respiratory symptoms. Occupational and Environmental Medicine, 56: 802-812.

Velasco, E., Pressley, S., Allwine, E., Westberg, H. and Lamb, B., 2005. Measurements of CO2 fluxes from the Mexico City urban landscape. Atmospheric Environment, 39: 7433-7446.
Widory, D. and Javoy, M., 2003. The carbon isotope composition of atmospheric CO2 in Paris. Earth and Planetary Science Letters, 215: 289-298.
Wood, F.B., 1988. Comment: On the need for validation of the Jones et al. temperature trends with respect to urban warming. Climate Change, 12: 297-312.
WRI, 1998. World Resources 1998-99: Environmental change and human health. Oxford University Press for the World Resources Institute.
Zimnoch, M., Florkowski, T., Necki, J.M. and Neubert, R.E.M., 2004. Diurnal variability of 13C and 18O of atmospheric CO2 in the urban atmosphere of Krakow, Poland. Isotopes in Environmental and Health Studies, 40: 129-143.

Wetzel, P. (2005): **Interannual and Decadal Variability in the Air-Sea Exchange of CO_2.**
Reports on Earth System Science, Max Planck Institute for Meteorology, No. 7/2004, pp. 77

Stier, P. (2005): **Towards the Assessment of the Aerosol Radiative Effects - A Global Modelling Approach.** Reports on Earth System Science, Max Planck Institute for Meteorology, No. 9/2004, pp. 111

Zuo, X. (2005): **Annual Hard Frosts and Economic Growth.**
Department of Economics, University of Hamburg, Hamburg, pp. 112

Jung, M. (2005): **Carbon sequestration options in the international climate regime.**
Department of Economics, University of Hamburg, Hamburg, pp. 119

Zhou, Y. (2005): **Economic Analysis of Selected Environmental Issues in China**
Department of Economics, University of Hamburg, Hamburg, pp. 101

Devasthale, A. (2005): **Aerosol Indirect Effect in the Thermal Spectral Range as Seen from Satellites**
Reports on Earth System Science, Max Planck Institute for Meteorology, No. 16/2005, pp. 70

Zandersen, M. (2005): **Aerosol Valuing Forest Recreation in Europe: Time and Spatial Considerations**
Department of Economics, University of Hamburg, Hamburg, pp. 125

Xuefeng Cui (2005***):*** **Interactions between Climate and Land Cover Changes on the Tibetan Plateau**
Reports on Earth System Science, Max Planck Institute for Meteorology, No. 17/2005, pp. 125

Stehfest, Elke (2005***):*** **Modelling of global crop production and resulting N_2O emissions**
Zentrum für Umweltsystemforschung Universität Kassel pp. 125

Kloster, Silvia (2006***):*** **DMS cycle in the ocean-atmosphere system and its response to anthropogenic perturbations.** Reports on Earth System Science, Max Planck Institute for Meteorology, No. 19/2006, pp. 82

Criscuolo, Luca (2006***):*** **Assessing the Agricultural System and the Carbon Cycle under Climate Change in Europe using a Dynamic Global Vegetation Model**
Reports on Earth System Science, Max Planck Institute for Meteorology, No. 21/2006, pp. 140

Tiwari, Yogesh Kumar (2006***):*** **Constraints of Satellite Derived CO_2 on Carbon Sources and Sinks**
Technical Reports, Max-Planck-Institut für Biogeochemie, No.7/2006, pp.125

Schurgers, Guillaume (2006***):*** **Constraints Long-term interactions between vegetation and climate - Model simulations for past and future -** Reports on Earth System Science, Max Planck Institute for Meteorology, No. 27/2006, pp. 135

Ronneberger, Kerstin Ellen (2006***):*** **The global agricultural land-use model KLUM - A coupling tool for integrated assessment -** Reports on Earth System Science, Max Planck Institute for Meteorology, No. 26/2006, pp. 123

Woth, Katja (2006***):*** **Regionalization of global climate change scenarios: An ensemble study of possible changes in the North Sea storm surge statistics**
Department for Earth Sciences, University of Hamburg, Hamburg, pp. 97

Hoelzemann, Judith Johanna (2006***):*** **Global Wildland Fire Emission Modeling for Atmospheric Chemistry Studies**
Reports on Earth System Science, Max Planck Institute for Meteorology, No. 28/2006, pp. 206

Gaslikova, Lidia (2006***):*** **High-resolution wave climate analysis in the Helgoland area**
Department for Earth Sciences, University of Hamburg, Hamburg, pp. 90

Grossmann, Iris (2006***):*** **Future perspectives for the Lower Elbe Region 2005–2030: Climate Trends and Globalisation**
GKSS-Forschungszentrum, Geesthacht, pp. 175

Narayan, Caroline (2006*)*: **CO2 fluxes and concentration patterns over Eurosiberia: A study using terrestrial biosphere models and the regional atmosphere model REMO**
Reports on Earth System Science, Max Planck Institute for Meteorology, No. 29/2006, pp. 242

Vizcaino, Miren (2006): **Long-term interactions between ice sheets and climate under anthropogenic greenhouse forcing Simulations with two complex Earth System Models**
Reports on Earth System Science, Max Planck Institute for Meteorology, No. 30/2006, pp. 187

Schwoon, Malte (2006): **Managing the Transition to Hydrogen and Fuel Cell Vehicles – Insights from Agent-based and Evolutionary Models –**
Reports on Earth System Science, Max Planck Institute for Meteorology, No. 32/2006, pp. 132

Link, Peter Michael (2006): **Modeling the economic impacts of changes in thermohaline circulation with an emphasis on the Barents Sea fisheries**
Reports on Earth System Science, Max Planck Institute for Meteorology, No. 33/2006, pp. 185

Li, Qian (2006): **Climatological analysis of planetary wave propagation in Northern Hemisphere winter**
Reports on Earth System Science, Max Planck Institute for Meteorology, No. 35/2006, pp. 153

Weis, Philipp (2006): **Ocean Tides and the Earth's Rotation - Results of a High-Resolving Ocean Model forced by the Lunisolar Tidal Potential**
Reports on Earth System Science, Max Planck Institute for Meteorology, No. 36/2006, pp. 115

Heistermann, Maik (2006): **Modelling the Global Dynamics of Rain-fed and Irrigated Croplands**
Reports on Earth System Science, Max Planck Institute for Meteorology, No. 37/2006, pp. 152